Available online at www.sciencedirect.com
ScienceDirect
Journal of Sound and Vibration 319 (2009) 768–794
JOURNAL OF SOUND AND VIBRATION
www.elsevier.com/locate/jsvi

Active structural acoustic control of repetitive impact noise

G. Pinte*, R. Boonen, W. Desmet, P. Sas

Department of Mechanical Engineering, Katholieke Universiteit Leuven, Celestijnenlaan 300B, B-3001 Heverlee, Belgium

Received 4 November 2007; received in revised form 6 July 2008; accepted 15 July 2008
Handling Editor: C.L. Morfey
Available online 2 September 2008

Abstract

This paper discusses the effectiveness of an Active Structural Acoustic Control (ASAC) system for the reduction of repetitive impact noise, radiated by structures with a high modal density in the controlled frequency range. Although there is a significant difference in nature between periodic and transient noise, up till now no specific research on ASAC of transient noise was reported. The development of the ASAC system is divided into two phases: the definition of the control configuration and the design of a suitable control algorithm. The optimal control configuration as well as the implemented control algorithm for the reduction of impact noise differ significantly from the common solutions in periodic noise control. In the first part of the paper, a practical methodology is presented to define a good control arrangement for transient noise control. The second part of the paper focuses on the design of control algorithms, adapted to the specific properties of impact noise. Since many industrial impact noise problems involve successive impacts with a repetitive behaviour, control algorithms with a learning behaviour are discussed. The efficiency of these Iterative Learning Control (ILC) algorithms is extensively demonstrated in this paper. The developed ASAC strategy has been verified on a thick steel plate, which is excited by successive impacts. The obtained results show that ASAC can be a very efficient transient noise control technique in certain industrial applications (e.g. presses, punching machines, etc.).

1. Introduction

Noise pollution from modern industrial activities is an environmental problem of growing importance. Especially in machine halls with production machines such as punching machines and presses, that generate impact noise, the radiated noise levels exceed often the legal regulations regarding human exposure to noise [1,2]. The noise, radiated by these machines, is mainly structure-borne, i.e. generated by structural vibrations of different mechanical parts. Various studies [3,4] have shown that Active Structural Acoustic Control (ASAC) has some potential to reduce stationary structure-borne noise. In ASAC the sound field radiated by a structure is controlled by intervening in the structural vibrations with actuators. Although there is a significant difference between periodic and transient noise, up till now almost no particular research on ASAC of transient noise has been reported, at least not to the authors' knowledge. The goal of the presented research is to study the possibilities of ASAC techniques to reduce transient structure-borne noise.

*Corresponding author. Tel.: +32 16 322536.
E-mail address: gregory.pinte@mech.kuleuven.be (G. Pinte).

0022-460X/$ - see front matter © 2008 Elsevier Ltd. All rights reserved.
doi:10.1016/j.jsv.2008.07.016

The efficiency of an ASAC system depends on the characteristics of the control actuators and sensors, on their configuration as well as on the implemented control algorithm. First of all, for the reduction of transient noise, actuators should be available, which can deliver the necessary energy levels within the required (short) time intervals. The physical arrangement of the control system defines the maximum achievable performance, while the controller design determines how close the practical system approximates this performance.

The first part of the paper describes a methodology to define the optimal control configuration. Based on experimental and simulation results, the best configuration for an optimal global performance of the practical ASAC system can be found.

In the second part of the paper, the algorithm for the control of the actuator(s) is designed. The existing ASAC control algorithms for the reduction of stationary noise can be classified into two groups: feedforward and feedback control algorithms. The standard adaptive feedforward algorithms [5] (e.g. filtered-x LMS algorithm), which are nowadays most popular in ASAC applications, cannot be used for the control of transient noise signals, since the adaptive part is often based on a continuous convergence to an optimum. Recently some new feedforward algorithms with specific adaptive filters [6] are proposed for the control of impulsive noise. Contrary to the conventional feedforward algorithms, the commonly used feedback algorithms developed for the control of continuous noise can be used for transient noise. However, the use of these feedback controllers is limited for practical, industrial applications: due to the high modal density of the controlled structures in the frequency range of interest, it is impossible to design efficient feedback controllers of limited order. Since in many industrial impact noise problems the successive impacts have a repetitive behaviour (e.g. a punching machine often performs the same operations several times), a learning behaviour can be introduced in the control algorithms, resulting in an improved performance of the controller as the number of controlled impacts increases. This paper presents the development of Iterative Learning Control (ILC) algorithms, which can be considered as adaptive feedforward algorithms. In an ILC controller the control signal is adapted to the specific repetitive properties of the transient noise from successive impacts. Because in industrial machinery, which radiates impact noise, advanced knowledge is often available of when the impact will occur, the ILC control filters can be noncausal: in this way the ILC controller can anticipate for a future impact. The advantages and drawbacks of causal and noncausal filtering in ILC algorithms are discussed in this paper. In the final ASAC controller, a combination of an ILC and a feedback algorithm is implemented, which is an example of a hybrid feedforward–feedback system as proposed in Refs. [7,8].

The last part of the paper presents the global noise reduction results, achieved by the developed ASAC systems. Several control configurations and algorithms are compared and the performance and the practical limitations of various strategies are discussed.

2. Demonstrator

In this paper, the developed ASAC strategies are used to cancel the low frequency (<1000 Hz) noise radiated by a thick free–free suspended plate (500 mm × 600 mm × 15 mm), which is excited by successive, repetitive impacts (Fig. 1). This set-up is studied, because its dynamic and acoustic behaviour resembles that of the massive frames of production machines, which radiate impact noise (e.g. punching machines, presses): the

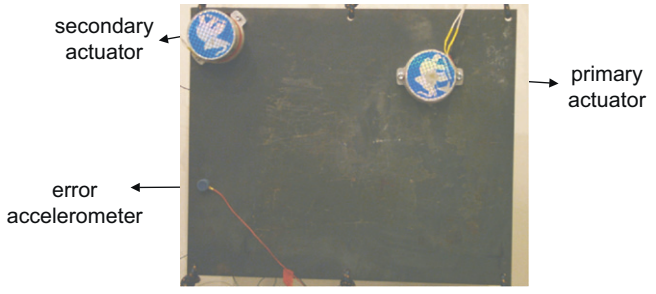

Fig. 1. The impact plate test setup with a primary disturbance and secondary control shaker and an error accelerometer.

Table 1
The resonance frequencies of the plate below 1000 Hz, defined by an experimental identification

Resonance number	1	2	3	4	5	6	7	8	9	10	11
Resonance frequency (Hz)	160	205	227	325	399	458	611	772	796	881	991

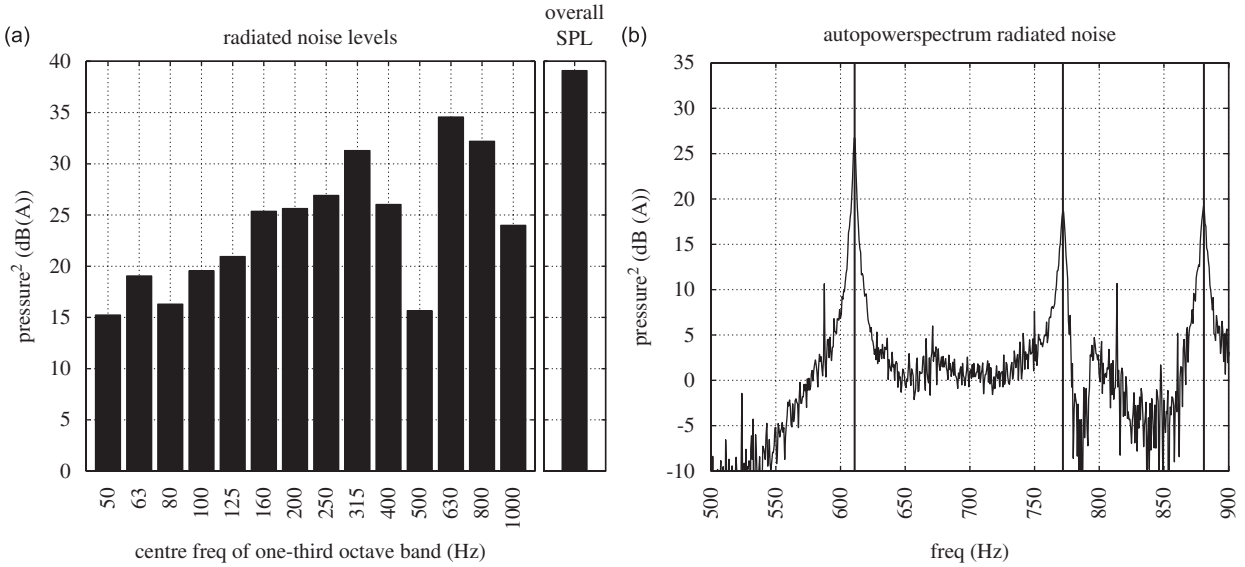

Fig. 2. The radiated noise, measured in the far field when the plate was excited by the primary shaker: (a) A-weighted noise levels in the one-third octave bands below 1000 Hz and A-weighted overall Sound Power Level and (b) detailed A-weighted autopowerspectrum between 500 and 900 Hz.

plate, which has a high modal density in the controlled frequency range below 1000 Hz (Table 1), radiates structureborne noise. A plate is an ideal demonstration breadboard since it is easy to define a reliable model to evaluate the theoretical possibilities of different ASAC controllers.

The disturbing impact forces on the plate are not caused by the actual collision of an object and the plate, but are simulated by a primary inertia shaker, generating force pulses on the plate with a duration of 2 ms. In this way, especially the low-frequency modes of the plate below 1000 Hz are excited, which is the frequency range to tackle by active means. Noise, which is radiated by the plate at higher frequencies, can be damped more efficiently by passive control techniques.

Since the successive input signals to the primary actuator are identical, the impact forces on the plate as well as the resulting vibrations and the radiated noise pulses are repetitive. The time between two consecutive impacts is variable but is always longer than 4 s such that the vibrations, due to a previous impact, are totally damped out when a new impact is generated. Consequently, the control of a new impact is not influenced by the previous impacts. Analogously to industrial machinery, where advanced knowledge is often available about the moment of the coming impact, in the demonstrator a trigger signal becomes active 0.5 s before a new voltage pulse is sent to the primary shaker.

Fig. 2(a) shows the A-weighted radiated noise levels in the one-third octave bands below 1000 Hz, which are measured in the far field when the plate is excited by the primary shaker. Most of the radiated acoustic energy is situated in the one-third octave bands with centre frequencies 630 and 800 Hz. A detailed autopowerspectrum of the radiated noise in this frequency range from 500 to 900 Hz is given in Fig. 2(b): the spectrum is mainly dominated by three efficiently radiating resonance frequencies of the plate (at 611, 772 and 881 Hz). Consequently the ASAC strategy should focus on noise reduction of the corresponding structural modes between 500 and 900 Hz.

3. Control configuration

The first phase in the development of an ASAC system is the definition of the optimal control configuration, i.e. the choice of the number and the location of actuator(s) and sensor(s). Many studies, both numerical and experimental, have already been devoted to this research topic. Two approaches can be distinguished, based on the goal function which is considered: some researchers minimize the vibration or acoustic level at certain locations, while others use vibration or acoustic power as cost function [9]. Simple problems (ASAC of beams [10], plates [11,12], etc.) can be described analytically such that different control configurations can be compared quite easily and some general design guidelines can be developed. Because the dynamic and acoustic behaviour of more complicated structures can only be evaluated by numerical models (e.g. finite element models, boundary element models, etc.) or extensive experimental models, the definition of the optimal control configuration demands computationally intensive optimisation algorithms (e.g. genetic algorithms [13,14]). Therefore, in many practical ASAC applications, the measuring/modelling and optimisation effort will be too high, even for a limited number of actuators and sensors. Consequently, simpler design rules, which can find sub-optimal but satisfactory configurations, are required. In this paragraph, a new methodology is presented to find suitable locations for actuators and sensors in the case of ASAC of impact noise. This methodology is a 2-step procedure, which first defines the actuator locations and afterwards searches compatible sensor locations.

Previous research [15] shows that, if a limited number of actuators and sensors is used, the optimal control arrangement is strongly frequency dependent. Since in the case of an impact excitation a broadband frequency range is excited, the performance of the control system should be balanced over this whole frequency range. In the excited frequency range, the structure will mainly vibrate and radiate noise at certain efficiently radiating resonance frequencies such that an efficient vibration reduction at these frequencies mainly determines the overall impact noise reduction and outweighs the control performance at other frequencies. Therefore, the actuators should be positioned at locations with a good controllability of the modes at these resonance frequencies. The controllability of different positions can be checked by calculating or measuring the resonance frequencies and corresponding mode shapes. The complexity of the structure and the impact duration, which defines the excited frequency range, determine the number of actuators required for a good vibration reduction. For the free–free suspended plate set-up, one actuator in a corner of the plate is sufficient, because all modes can be excited in this position. Also in the considered practical applications, one actuator is often sufficient to suppress the most efficiently radiating resonance frequencies, e.g. in a punching machine one actuator in a corner of the frame can control the most efficiently radiating structural modes.

The second part in the definition of the control configuration is the selection of the sensor locations. For arbitrary sensor positions, resonances as well as anti-resonances appear in the transfer function between the actuator and the sensor. The resonance frequencies are identical for all the possible sensor locations, while the anti-resonance frequencies strongly depend on the sensor position. At a resonance frequency, the plate response to a force is dominated by one mode shape and a large vibration reduction at the error sensor will result in a global reduction of the plate vibrations. At an off-resonance frequency, the plate response is governed by several modes, and a good vibration reduction at the error sensor will not necessarily result in a global reduction. Especially at an anti-resonance frequency of the actuator–sensor transfer function, a high force will be generated by the secondary actuator to create a good vibration reduction at the sensor location. However, since an anti-resonance is not a global property of the plate, this high force will cause high vibration levels at the greater part of the plate and the global vibration level will be amplified instead of being reduced.

It is clear that, when there are anti-resonances in the actuator–sensor transfer function, the local impact disturbance rejection at the error sensor does not result in a good global performance. This problem can be solved by an optimal choice of the control algorithm or by a suitable selection of the control configuration. A control algorithm should be developed which only cancels the error sensor vibrations at the resonance frequencies without sending a control signal at the intermediate anti-resonance frequencies. In this way, the resonance frequencies can be damped, resulting in a global vibration reduction at these frequencies, while the response at the anti-resonance frequencies is unaltered. Unless a very specific collocated control configuration is used (see the next section), the required control algorithm will be very complicated for systems with a high modal density in the controlled frequency range. A second solution is the avoidance of anti-resonances in the

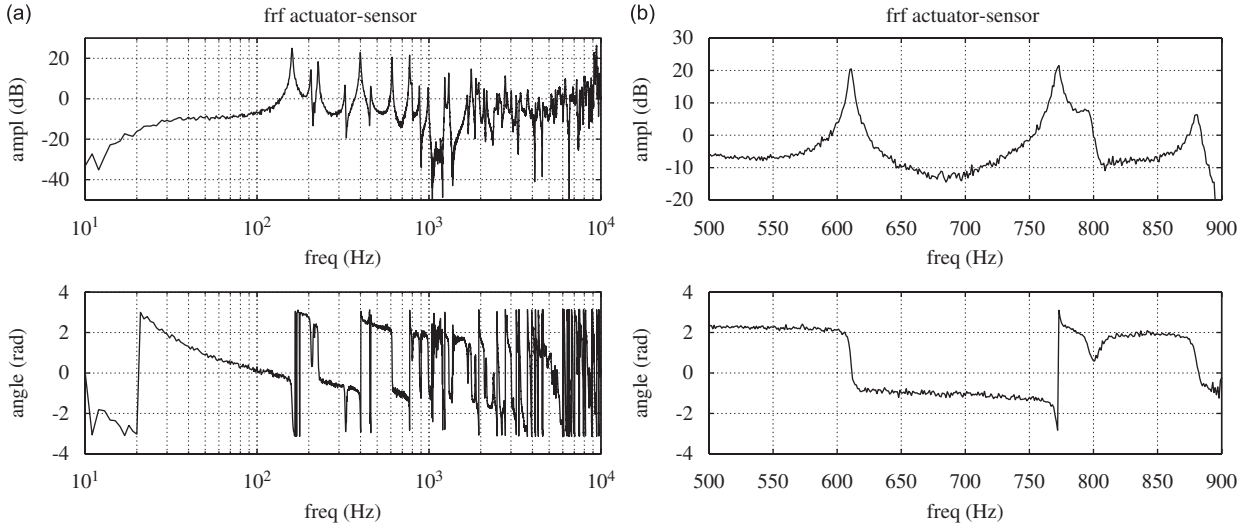

Fig. 3. The transfer function between the actuator force and the sensor: (a) over the whole frequency range and (b) in the frequency range 500–900 Hz, where the greatest noise reduction is required.

transfer function between the actuator and the sensor. The position of the error sensor on the plate is defined according to this second solution. Since most of the acoustic energy is radiated between 500 and 900 Hz (Section 2), the ASAC strategy should focus on a noise reduction in this frequency range. Therefore the error sensor should be positioned such that, between 500 and 900 Hz, all the efficiently radiating modes can be observed and the number of zeros in the transfer function between the actuator force and the sensor response is as small as possible. Forty possible error sensor positions have been compared experimentally. After measuring the transfer functions between the secondary actuator and all these possible sensor positions, the observability of the efficiently radiating modes between 500 and 900 Hz is checked for each sensor. The sensor locations with a limited observability of one or more modes are no longer retained. Afterwards, the number of zeros between 500 and 900 Hz are defined for the remaining transfer functions. A few locations can be found with only one zero in this frequency range. Out of these locations, the sensor, corresponding with the highest minimum value of the transfer function between 500 and 900 Hz, is selected. This position, which is used in the practical experiments, is also indicated in Fig. 1. The transfer function between the actuator force and the sensor response at this position is shown in Fig. 3(a). A more detailed representation of the frequency range between 500 and 900 Hz is plotted in Fig. 3(b): it is clear that all the efficient radiating modes are present and that only one zero around 800 Hz (with sufficient damping) occurs in this transfer function. Consequently, if a control algorithm can be designed, which cancels the disturbance at this error sensor, this will result in a global reduction of the radiated noise. The design of such algorithm is the subject of the following section.

4. Iterative learning control

4.1. Introduction

The second step in the design of an ASAC system, after the selection of a suitable control configuration, is the implementation of an efficient controller, which processes the sensor information to send a control signal to the actuator(s). Because the conventional feedback and feedforward ASAC control algorithms for the reduction of stationary noise are not suitable in this application (due to respectively the high modal density of the radiating structure and the transient character of the disturbance), an iterative learning control (ILC) algorithm is applied in the presented ASAC controller for the plate. ILC is a relatively new area of study in control theory, very suitable to cancel repetitive disturbances [16].

The ILC approach was motivated by the intuitive idea that it should be possible to improve the performance of a system that performs repetitively the same task and reproduces continuously the same error (welding robots, pick-and-place machines, etc.). Using the experience from the past, modifications to the input signal can be applied to the system during the next operation in order to obtain a better future performance. The first contribution on ILC, a paper by Uchiyama [17], was not widely known, because it was only published in Japanese. The idea of ILC was further developed by Arimoto [18,19], mainly active in the field of robotics, and became also popular among other researchers (Longman [20], Horowitz [21], etc.). A good survey of ILC can be found in the book of Moore [22] and a more recent overview paper [23]. Longman [20] presents some practical ILC design rules for engineering applications. In a recent paper by Goldsmith [24] it was shown that ILC was not fundamentally different from time-invariant control methods. He proves that causal ILC can do no better than conventional feedback control and suggests that future work on ILC should focus on the benefits of noncausal ILC filters. The practical usefulness of a noncausal ILC system will be demonstrated extensively in this section. Although the potential of ILC was demonstrated for a broad class of applications during the last two decades, the technique has only very recently been used in the field of ANC [25] and ASAC [26]. In both papers, the results obtained by the ILC controller are superior compared to those achieved by conventional feedback and feedforward control methods.

4.2. Theoretical background

The plate system, that is controlled in this paper, is considered to be linear time-invariant and causal and is described by the following system description:

$$y(k) = P_{\text{sec}}(\text{D})u(k) + P_{\text{dist}}(\text{D})d(k) \tag{1}$$

with

- D the unit delay operator ($\text{D}x(k) = x(k+1)$)
- $P_{\text{sec}}(\text{D})$ the discrete operator, which defines the relation between the input signal to the secondary actuator and the signal measured by the error accelerometer
- $P_{\text{dist}}(\text{D})$ the discrete operator, which defines the relation between disturbing impact force and the signal measured by the error accelerometer
- $y(k)$ the signal measured by the error accelerometer at time interval k
- $u(k)$ the control signal sent to the secondary actuator at time interval k
- $d(k)$ the disturbing impact force at time interval k

Since separate impacts are studied, which generate transient vibrations in the plate, several discrete time intervals with a fixed duration (p time steps) can be studied separately. A trigger signal, which announces a new impact and defines the beginning k_i of a new time interval, is supposed to be available. Define the p step histories of the error signal, the control signal and the disturbance force at the ith impact according to:

$$\mathbf{y}_i = [y_i(0)\ \ y_i(1)\ \ \ldots\ \ y_i(p-1)]^{\text{T}} \tag{2}$$

$$\mathbf{u}_i = [u_i(0)\ \ u_i(1)\ \ \ldots\ \ u_i(p-1)]^{\text{T}} \tag{3}$$

$$\mathbf{d}_i = [d_i(0)\ \ d_i(1)\ \ \ldots\ \ d_i(p-1)]^{\text{T}} \tag{4}$$

with

$$y_i(k) = y(k_i + k) \tag{5}$$

$$u_i(k) = u(k_i + k) \tag{6}$$

$$d_i(k) = d(k_i + k) \tag{7}$$

Because the successive disturbing impact forces are supposed to be repetitive, all the time series $\mathbf{d}_i$ are equal to $\mathbf{d}$. Using Eqs. (2)–(4), the system description Eq. (1) can be posed in a matrix form:

$$\mathbf{y}_i = \mathbf{P}_{\text{sec}}\mathbf{u}_i + \mathbf{P}_{\text{dist}}\mathbf{d}_i \tag{8}$$

with

$$\mathbf{P}_{\text{sec}} = \begin{bmatrix} h_{P_{\text{sec}}}(0) & 0 & \dots & 0 \\ h_{P_{\text{sec}}}(1) & h_{P_{\text{sec}}}(0) & & \vdots \\ \vdots & & \ddots & 0 \\ h_{P_{\text{sec}}}(p-1) & h_{P_{\text{sec}}}(p-2) & \dots & h_{P_{\text{sec}}}(0) \end{bmatrix} \tag{9}$$

and

$$\mathbf{P}_{\text{dist}} = \begin{bmatrix} h_{P_{\text{dist}}}(0) & 0 & \dots & 0 \\ h_{P_{\text{dist}}}(1) & h_{P_{\text{dist}}}(0) & & \vdots \\ \vdots & & \ddots & 0 \\ h_{P_{\text{dist}}}(p-1) & h_{P_{\text{dist}}}(p-2) & \dots & h_{P_{\text{dist}}}(0) \end{bmatrix} \tag{10}$$

where $h_{P_{\text{sec}}}(k)$ and $h_{P_{\text{dist}}}(k)$ are the discrete impulse responses of the operators $P_{\text{sec}}(\text{D})$ and $P_{\text{dist}}(\text{D})$.

In this paper, a first order, trial-invariant ILC algorithm, which is represented in Fig. 4, is applied. In first-order ILC, the control signal for a new impact $\mathbf{u}_i$ only depends on the control signal $\mathbf{u}_{i-1}$ and the remaining error signal $\mathbf{y}_{i-1}$ at the previous impact, while in higher-order ILC [27,28] the control and error signals of earlier impacts $\mathbf{u}_{i-2}$, $\mathbf{y}_{i-2}$, $\mathbf{u}_{i-3}$, $\mathbf{y}_{i-3}$, etc. can also influence the control signal $\mathbf{u}_i$. The control filters are supposed to be trial-invariant, which means that the control law between the input signals $\mathbf{u}_{i-1}$ and $\mathbf{y}_{i-1}$ and the calculated ILC control signal $\mathbf{u}_i$ is invariant over all impacts. The ILC control law, applied in the developed control algorithms, is linear: the control signal for the new impact $\mathbf{u}_i$ is a linear combination of the previous control signal $\mathbf{u}_{i-1}$ and the error signal $\mathbf{y}_i$, measured at the previous impact:

$$\mathbf{u}_i = \mathbf{Q}\mathbf{u}_{i-1} + \mathbf{L}\mathbf{y}_{i-1} \tag{11}$$

with

$\mathbf{Q}$, $\mathbf{L}$: $p \times p$-matrices

In most applications, $\mathbf{Q}$, which relates the control signal for the new impact $\mathbf{u}_i$ to the previous control signal $\mathbf{u}_{i-1}$, is a diagonal matrix with constant coefficients, mostly equal to 1. $\mathbf{L}$, which defines the relation between the new control signal $\mathbf{u}_i$ and the error signal at the previous impact $\mathbf{y}_{i-1}$, determines the stability of the ILC algorithm. In case of causal ILC, $\mathbf{L}$ is lower triangular, which means that a time sample of the new control signal $\mathbf{u}_i(n)$ is only influenced by earlier samples of the error at the previous impact $\mathbf{y}_{i-1}(n)$, $\mathbf{y}_{i-1}(n-1)$, $\mathbf{y}_{i-1}(n-2)$, etc. Since ILC is an offline method, which processes the data from a previous impact to calculate the control signal for the new impact, also noncausal operators can be used in the design of ILC filters. Fig. 5 shows how these noncausal operators can use 'future' time samples from a previous impact ($\mathbf{y}_{i-1}(n+1)$, $\mathbf{y}_{i-1}(n+2)$, etc.) to calculate the current control action. Due to this noncausal filtering, the ILC controller can anticipate for a new impact, announced by the trigger signal. In this paper, the benefits of noncausal ILC are investigated, allowing $\mathbf{L}$ to be a full matrix of learning gains.

The ILC system, described by Eq. (11), will be bounded-input, bounded-output stable, if the magnitudes of all the eigenvalues of $\mathbf{Q} - \mathbf{P}_{\text{sec}}\mathbf{L}$ are less than 1 [29]:

$$|\lambda_s(\mathbf{Q} - \mathbf{P}_{\text{sec}}\mathbf{L})| < 1 \quad \forall s \tag{12}$$

When this condition is fulfilled, the error signal converges to

$$\mathbf{y}_\infty = (\mathbf{I} - \mathbf{Q} - \mathbf{P}_{\text{sec}}\mathbf{L})^{-1}(\mathbf{I} - \mathbf{Q})\mathbf{P}_{\text{dist}}\mathbf{d} \tag{13}$$

It is important to notice that the error signal can only become 0 if $\mathbf{Q} = \mathbf{I}$. This is the reason why most of the proposed ILC schemes operate with $\mathbf{Q} = \mathbf{I}$.

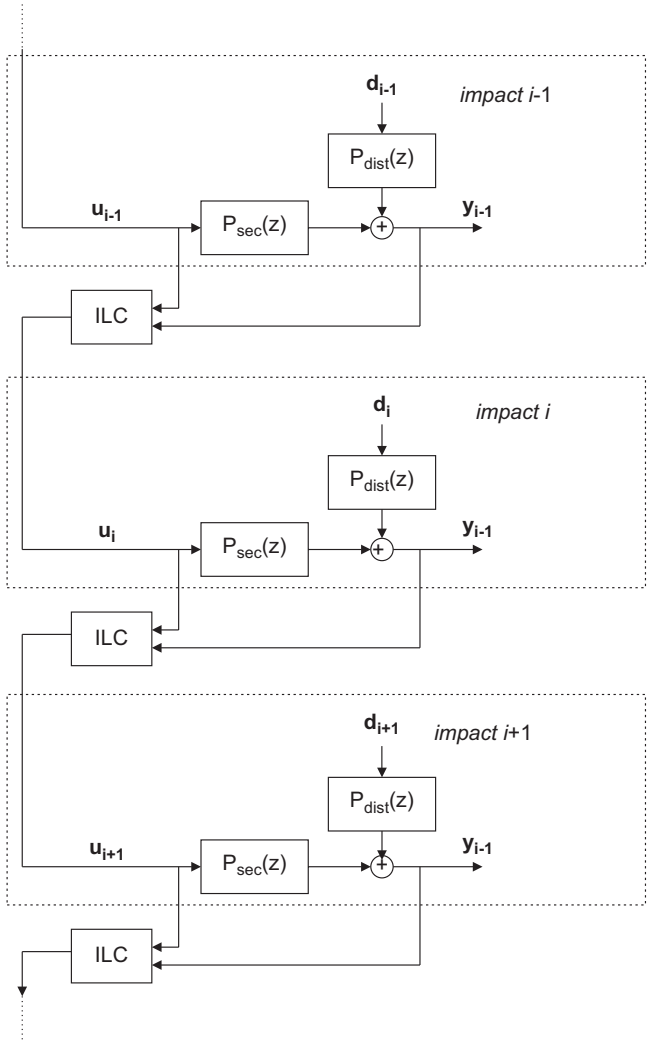

Fig. 4. Control scheme of first order, trial-invariant ILC.

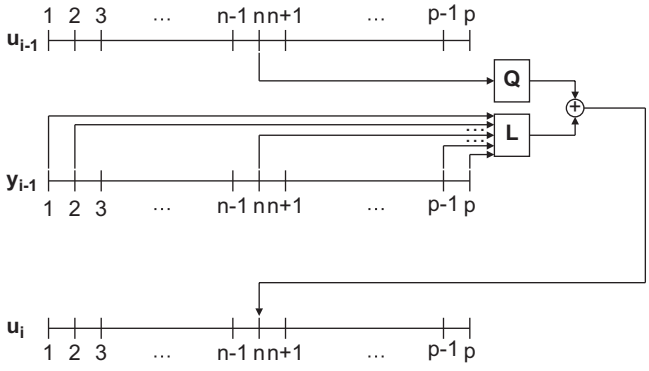

Fig. 5. The use of a noncausal operator L in the ILC design.

In the remainder of this paper, $\mathbf{Q}$ is supposed to be diagonal with constant coefficients q and $\mathbf{L}$ is supposed to be the matrix representation of a noncausal time-invariant difference equation with transfer function $L(z)$:

$$\mathbf{Q} = q\mathbf{I} \tag{14}$$

and

$$\mathbf{L} = \begin{bmatrix} h_L(0) & h_L(-1) & h_L(-2) & \dots & h_L(-(p-1)) \\ h_L(1) & h_L(0) & h_L(-2) & & h_L(-(p-2)) \\ h_L(2) & h_L(1) & h_L(0) & & h_L(-(p-3)) \\ \vdots & & & \ddots & \vdots \\ h_L(p-1) & h_L(p-2) & h_L(p-3) & \dots & h_L(0) \end{bmatrix} \tag{15}$$

where $h_L(k)$ is the discrete impulse response of $L(z)$.

Analogous to this expression, $\mathbf{Q}$ can be interpreted as the matrix representation of a difference equation with transfer function $Q(z) = q$.

Although stability and convergence can be obtained by fulfilling condition Eq. (12), the practical usefulness of this formula is very limited. Since a monotonic convergence is not guaranteed, the transient behaviour of the ILC algorithm can be undesirable. The poor transient behaviour of some ILC algorithms, although complying to Eq. (12), is clearly illustrated in Ref. [20]: it is possible that a disturbance has first grown to undesirably high levels during the first impacts before it is ultimately canceled after a high number of impacts. To assure good transients, a criterion for monotonic convergence is required. The following condition, formulated in the frequency domain, guarantees a monotonic decay of the amplitudes of all the frequency components [20]:

$$|q - L(\mathrm{e}^{\mathrm{i}\omega T})P_{\mathrm{sec}}(\mathrm{e}^{\mathrm{i}\omega T})| < 1 \tag{16}$$

with

T	the sampling time
ω	the angular frequency
$L(\mathrm{e}^{\mathrm{i}\omega T})$	the discrete Fourier transform of L
$P_{\mathrm{sec}}(\mathrm{e}^{\mathrm{i}\omega T})$	the discrete Fourier transform of P_{sec}

This criterion indicates that the Nyquist curve of $L(\mathrm{e}^{\mathrm{i}\omega T})P_{\mathrm{sec}}(\mathrm{e}^{\mathrm{i}\omega T})$ has to be located inside a unit circle with the center point $(q, 0)$, commonly denoted as the learning circle. Although this formula is only correct for a steady-state response, Longman shows in Ref. [20] that it is also a good condition to get a reduction of the transient response.

In the design of the ILC control matrices $\mathbf{Q}$ and $\mathbf{L}$, developed for the control of the plate, a trade-off has to be made between performance (Eq. (13)) and stability (Eq. (16)). Therefore the following design procedure is suggested:

(1) The transfer function between the secondary actuator and the error sensor is measured.
(2) The control filter $L(z)$ is shaped such that, in the frequency range where control performance is required,
   - the phase of $L(\mathrm{e}^{\mathrm{i}\omega T})P_{\mathrm{sec}}(\mathrm{e}^{\mathrm{i}\omega T})$ stays between -90° and 90° to assure stability (Eq. (16) with $q \approx 1$) and
   - the maximum amplitude of $L(\mathrm{e}^{\mathrm{i}\omega T})P_{\mathrm{sec}}(\mathrm{e}^{\mathrm{i}\omega T})$ is almost equal to 1 to guarantee performance (Eq. (13)).
(3) A bandpass filter is added to the $L(z)$-filter for stability reasons such that the amplitude of $L(\mathrm{e}^{\mathrm{i}\omega T})P_{\mathrm{sec}}(\mathrm{e}^{\mathrm{i}\omega T})$ decreases significantly outside the frequency range of interest, where the -90° and 90°-phase limits are exceeded.
(4) The last phase in the ILC design, is the definition of q, which should be chosen as close as possible to 1 for a good performance (Eq. (13)): if for $q = 1$ the Nyquist curve of $L(\mathrm{e}^{\mathrm{i}\omega T})P_{\mathrm{sec}}(\mathrm{e}^{\mathrm{i}\omega T})$ goes outside the learning circle, a slightly smaller value should be chosen for q to introduce robustness in the control algorithm.

4.3. Practical implementation

Two ILC algorithms are discussed in the remainder of this section. First a causal ILC algorithm is presented to show the equivalence of this algorithm with time-invariant feedback control algorithms and to indicate the limitations in the design of the ILC controller when only causal filters are used. In the second example, the interesting benefits of noncausal ILC filters are exploited. In all the experiments, the secondary actuator is an inertia shaker and the error sensor is an accelerometer.

4.3.1. Example 1: causal ILC

Due to the high modal density of the plate in the controlled frequency range, it is impossible to design a stable causal control algorithm of limited order for the optimal control arrangement, defined in the previous section. Therefore, the causal algorithm is implemented for a collocated control configuration, where the actuator as well as the sensor are placed in the same corner of the plate. This collocated configuration with a dual actuator and sensor pair results in some very attractive stability properties, i.e. alternating poles and zeros in the secondary plant transfer function P_{sec} (Fig. 6).

The control matrices $\mathbf{Q}$ and $\mathbf{L}$ are designed according to the aforementioned methodology. First, the L-filter was shaped. In the lower frequency range, the phase of P_{sec} can be easily compensated by a negative phase of the L-filter to keep the phase of LP_{sec} between -90° and 90°. The gain of L is adjusted such that the maximum amplitude of LP_{sec} is close to 1 in this lower-frequency range. In the higher frequency range (above 500 Hz), it is impossible to design a causal L-filter, which compensates the phase loss of P_{sec} caused by a time delay. Consequently, for robustness, a lowpass filter should be introduced in L to decrease the amplitude of LP_{sec} at the higher frequencies, where the phase of LP_{sec} exceeds the $(-90^\circ, 90^\circ)$-limits. This results in the following L-filter (Fig. 7(a)):

$$L = \frac{-30}{s + 2\pi 60} \tag{17}$$

This filter was developed in the continuous domain and afterwards transformed to the discrete domain using Tustin's transformation rule. Since for $q = 1$ the Nyquist curve of LP_{sec} exceeds the learning circle, q has to be reduced to 0.97. Fig. 7(b) shows that for this value of q the stability condition for monotonic convergence Eq. (16) is fulfilled.

The reduction $|Y_\infty(e^{i\omega T})|/|P_{\text{dist}}(e^{i\omega T})D(e^{i\omega T})|$, which can be theoretically obtained by the implementation of the developed ILC algorithm, is evaluated using Eq. (13) and is shown in Fig. 8 ($Y_\infty(e^{i\omega T})$ and $D(e^{i\omega T})$ are the

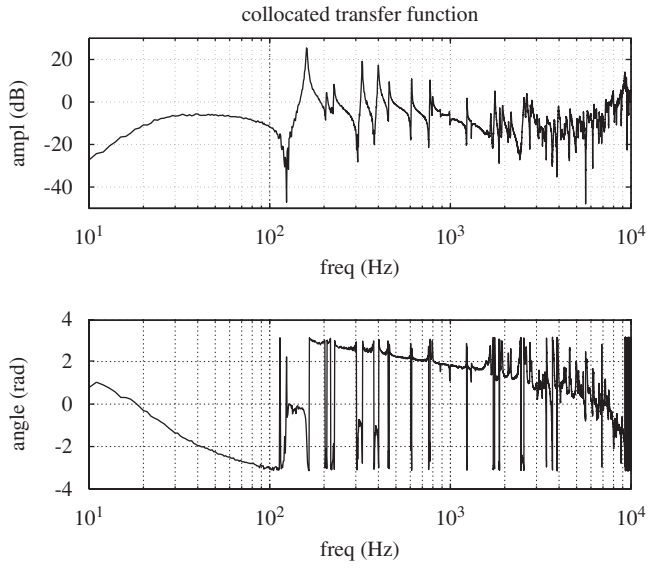

Fig. 6. The transfer function P_{sec} between the collocated actuator force and the accelerometer signal.

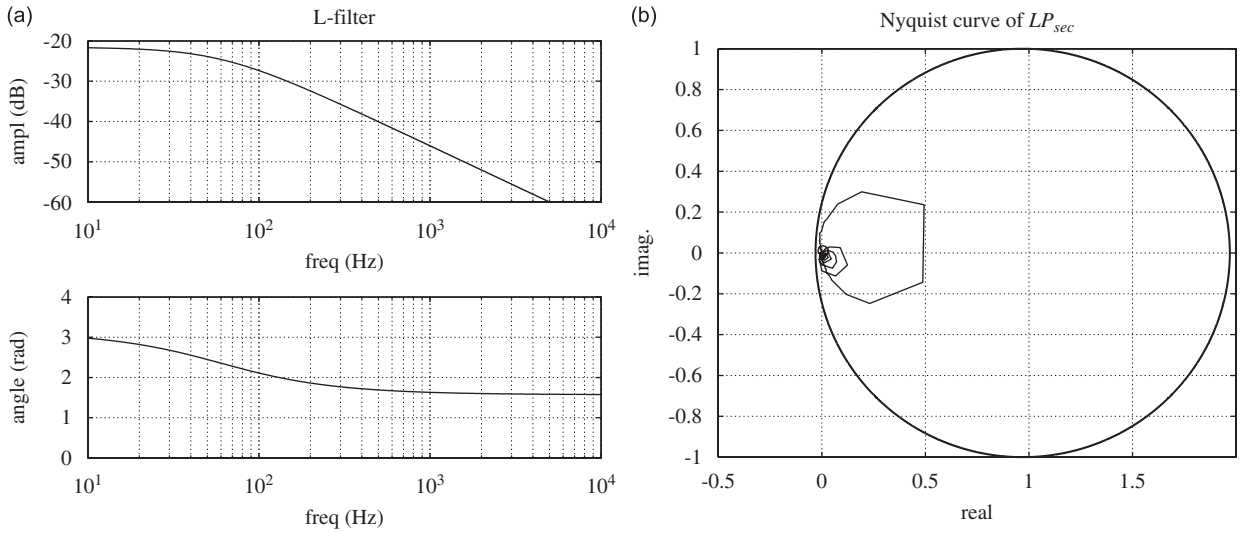

Fig. 7. The design of the control filters Q and L: (a) the transfer function of the L-filter and (b) the Nyquist plot of LP_{sec} inside the learning circle (the stability test for $q = 0.97$).

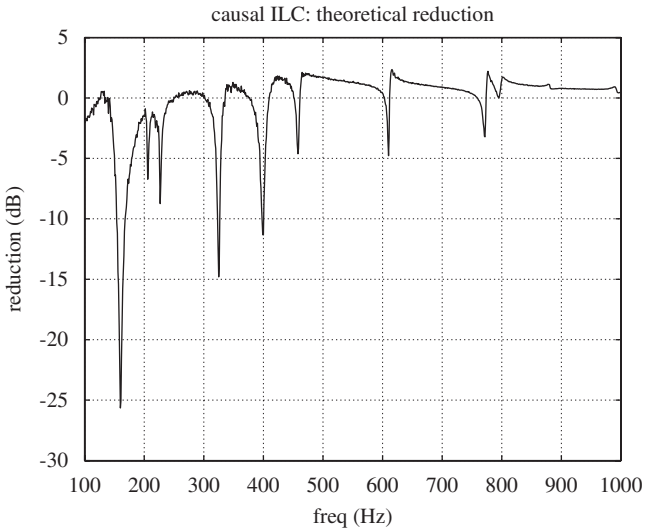

Fig. 8. The theoretical reduction $|Y_\infty(e^{i\omega T})|/|P_{\mathrm{dist}}(e^{i\omega T})D(e^{i\omega T})|$, which can be achieved by the causal ILC controller as well as by the equivalent time-invariant feedback controller.

discrete Fourier transform of y_∞ and d, respectively). The greatest theoretical reduction can be achieved at the resonance frequencies of the plate, while there is no reduction at the intermediate frequencies. According to Eq. (13), the final error at the sensor will be only small, if $P_{\mathrm{sec}}L$ is high compared to $I - Q$. Since the alternating poles and zeros of P_{sec} are not compensated by the L-filter, $P_{\mathrm{sec}}L$ will only be high enough at the poles of P_{sec} to create a vibration reduction. At the intermediate frequencies between the poles, no control signal will be sent to the secondary actuator and the vibration pattern is unaltered. Due to the lowpass characteristic of the ILC filter L, the frequency band in which reduction can be obtained at the error sensor is limited: the error can only be reduced by more than 5 dB at the resonance peaks of the plate below 450 Hz. It is also important to notice that this low-frequency performance does not result in a deterioration in the higher frequency range.

Goldsmith [24] and Verwoerd [30] state that for causal ILC filters Q and L an equivalent time-invariant feedback controller exists, which yields the same theoretical reduction at the error sensor (Fig. 8). This equivalent feedback controller can be defined as

$$\mathbf{C}_{\mathrm{FB}} = (\mathbf{I} - \mathbf{Q})^{-1}\mathbf{L} \tag{18}$$

In this application, the resulting equivalent controller becomes

$$C_{\mathrm{FB}} = \frac{L}{1-q} = \frac{-30}{0.03(s + 2\pi 60)} \tag{19}$$

The performance of the ILC controller is practically compared with the time-invariant feedback controller on the plate set-up. Both algorithms are implemented on a dSPACE 1103 DSP board, which calculates the control signals for the secondary actuator. Fig. 9(a) shows the error signals in the time domain, when the plate is excited by a primary impact force. The different curves compare the remaining error signals, which are obtained by the ILC algorithm after a different number of impacts. During the first 80 impacts, the error acceleration, caused by the primary shaker, becomes significantly smaller at each impact, due to the updated ILC control force. This learning behaviour can also be observed in Fig. 9(b): there is a clear reduction of the error signal in the lower frequency range between 50 and 250 Hz during the first 80 impacts. After the 80th impact, the ILC algorithm has converged and there is no further improvement at the consecutive pulses. While the vibration reduction is significant in the lower frequency, the ILC algorithm has no influence on the error signal in the higher frequency range. This behaviour was exactly predicted by the theoretical formula in Eq. (13), as was explained above.

Contrary to the ILC controller, the performance of the time-invariant feedback controller is equal for all the controlled impact disturbances. The reduction achieved by this time-invariant controller is plotted in Fig. 10 and compared to the reduction obtained by the ILC controller after convergence. It is clear that the time-invariant feedback controller can achieve the same error after one impact as the ILC controller obtains only after convergence, which requires a large number of learning impacts. This result shows that it is useless to apply a causal learning controller, which requires a certain number of impacts to update the control signal before convergence is achieved. Another disadvantage of the ILC algorithm, which can be avoided by applying a time-invariant feedback algorithm, is the necessity of an accurate trigger signal to predict the next impact: while the time-invariant controller is permanently active, the ILC controller only sends a control signal to the secondary actuators, when a new impact is announced by a trigger signal. Since this example

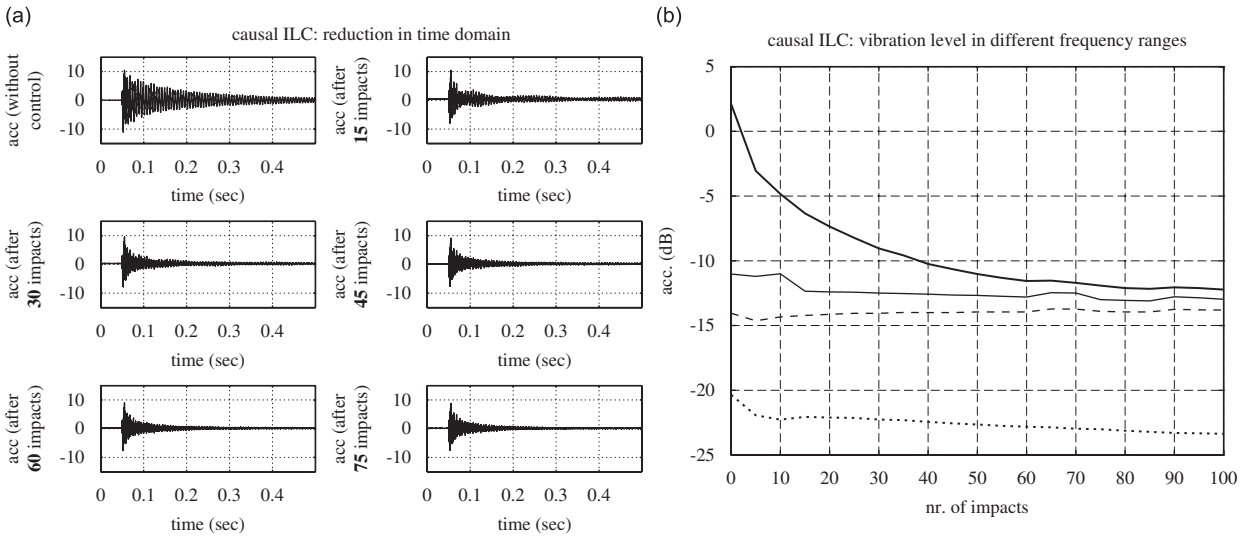

Fig. 9. The performance of the causal ILC controller: (a) the error acceleration after a certain number of learning impacts (shown in the time domain) and (b) the error acceleration as a function of the number of learning impacts (shown in different frequency bands: 50–250 Hz (bold line), 250–500 Hz (dotted line), 500–750 Hz (solid line) and 750–1000 Hz (dashed line)).

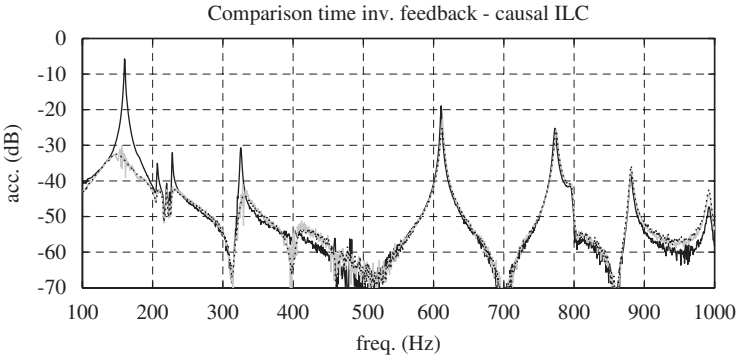

Fig. 10. The remaining error signal, measured by the error accelerometer, without control (bold line), with feedback control (dotted line) and with ILC after convergence (grey line).

shows that there is no reason to use causal ILC instead of time-invariant feedback control, in the following paragraphs the possibilities of noncausal ILC are investigated.

4.3.2. Example 2: noncausal ILC

In this paragraph, a noncausal ILC algorithm is designed for the control of the optimal sensor–actuator configuration, which was selected in Section 3. The transfer function of the secondary plant P_{sec} for this control arrangement is shown in Fig. 3(a). The control matrices $\mathbf{Q}$ and $\mathbf{L}$ are again designed according to the methodology, presented in the first part of this section. The frequency range, where control performance is desired, is situated between 500 and 900 Hz. Since in this range the phase of LP_{sec} should stay between -90° and 90°, the phase lag of 540° in P_{sec} between 500 and 900 Hz caused by 4 poles and only 1 zero should be compensated by 3 zeros in the control filter L, which are placed at 620, 780 and 880 Hz. In order to limit the high-frequency amplification of L, each zero in the controller is compensated by a pole. Therefore 3 poles at frequencies higher than 900 Hz are introduced in L (1 pole at 900 Hz and 2 poles at 5000 Hz). This results in the following controller L_1:

$$L_1 = L_{1,a}L_{1,b}L_{1,c} \tag{20}$$

with

$$L_{1,a} = \frac{900^2}{620^2}\frac{s^2 + 2\times 0.01(2\pi 620)s + (2\pi 620)^2}{s^2 + 2\times 0.03(2\pi 900)s + (2\pi 900)^2} \tag{21}$$

$$L_{1,b} = \frac{5000^2}{780^2}\frac{s^2 + 2\times 0.01(2\pi 780)s + (2\pi 780)^2}{s^2 + 2\times 0.03(2\pi 5000)s + (2\pi 5000)^2} \tag{22}$$

$$L_{1,c} = \frac{5000^2}{880^2}\frac{s^2 + 2\times 0.03(2\pi 880)s + (2\pi 880)^2}{s^2 + 2\times 0.03(2\pi 5000)s + (2\pi 5000)^2} \tag{23}$$

Due to the 3 poles between 500 and 900 Hz, the phase of LP_{sec} stays inside a band of 180° in this frequency range. To shift this 180°-band between -90° and 90°, a second compensator has been added to L_1:

$$L_2 = L_1\frac{2\pi 50}{s + 2\pi 50}\frac{s^2 + 2\times 0.4(2\pi 1000)s + (2\pi 1000)^2}{s^2 + 2\times 0.4(2\pi 2000)s + (2\pi 2000)^2} \tag{24}$$

Figs. 11(a and b) show the transfer functions of L_2 and L_2P_{sec}. It is clear that, in the frequency range of interest (500–900 Hz), the phase of L_2P_{sec} stays between -90° and 90°. The developed L_2-filter is still causal, the benefits of noncausality are only used in the second phase of the controller design. Two noncausal bandpass filters L_3 and L_4 are added to L_2 to create L such that the amplitude of LP_{sec} decreases significantly outside the frequency range of interest without any phase change. L_3 consists of a noncausal lowpass filter $L_{3,\text{lp}}$

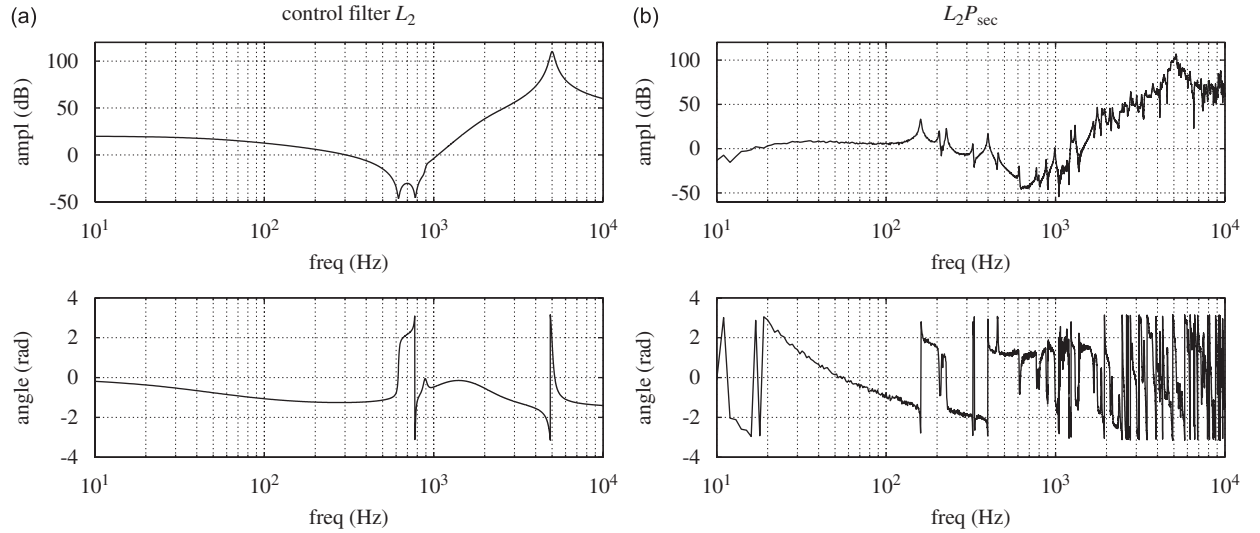

Fig. 11. The first part in the design of the ILC filter for the control of the optimal control configuration: the transfer functions of (a) the ILC control filter L_2 and (b) $P_{sec}L_2$.

and a noncausal highpass filter $L_{3,hp}$. Since a strong roll-off is necessary to decrease the amplitude of LP_{sec} sufficiently outside the frequency range 500–900 Hz, these both filters are of 12th order (the actual implementation of these noncausal filters is explained in Appendix A). In both filters, the phase lag due to a causal pole is compensated by the phase lead due to an anti-causal pole (an anti-causal system does not process earlier samples from a previous impact but only uses future time samples to calculate the current control action):

$$L_3 = L_{3,lp}L_{3,hp} \tag{25}$$

with

$$L_{3,lp} = \left(\frac{(2\pi 600)^4}{(s^2 + 2\times 0.4(2\pi 600)s + (2\pi 600)^2)(s^2 - 2\times 0.4(2\pi 600)s + (2\pi 600)^2)}\right)^3 \tag{26}$$

$$L_{3,hp} = \left(\frac{s^4}{(s^2 + 2\times 0.4(2\pi 800)s + (2\pi 800)^2)(s^2 - 2\times 0.4(2\pi 800)s + (2\pi 800)^2)}\right)^3 \tag{27}$$

Finally, a second noncausal compensator L_4 was also implemented in the ILC control filter L ($= L_2L_3L_4$) to create some extra robustness. The compensator L_4 consists of 2 causal (both at 700 Hz) and 2 anti-causal (also at 700 Hz) poles as well as 2 causal (at 400 and 1200 Hz) and 2 anti-causal zeros (also at 400 and 1200 Hz). This further increases the amplitude of LP_{sec} between 500 and 900 Hz and reduces its amplitude just below and above this frequency range, again without any phase change.

$$L_4 = \frac{L_{zero,1}L_{zero,2}}{L_{pole}^2} \tag{28}$$

with

$$L_{zero,1} = (s^2 + 2\times 0.05(2\pi 400)s + (2\pi 400)^2)(s^2 - 2\times 0.05(2\pi 400)s + (2\pi 400)^2) \tag{29}$$

$$L_{zero,2} = (s^2 + 2\times 0.1(2\pi 1200)s + (2\pi 1200)^2)(s^2 - 2\times 0.1(2\pi 1200)s + (2\pi 1200)^2) \tag{30}$$

$$L_{pole} = \frac{1}{(s^2 + 2\times 0.3(2\pi 700)s + (2\pi 700)^2)(s^2 - 2\times 0.3(2\pi 700)s + (2\pi 700)^2)} \tag{31}$$

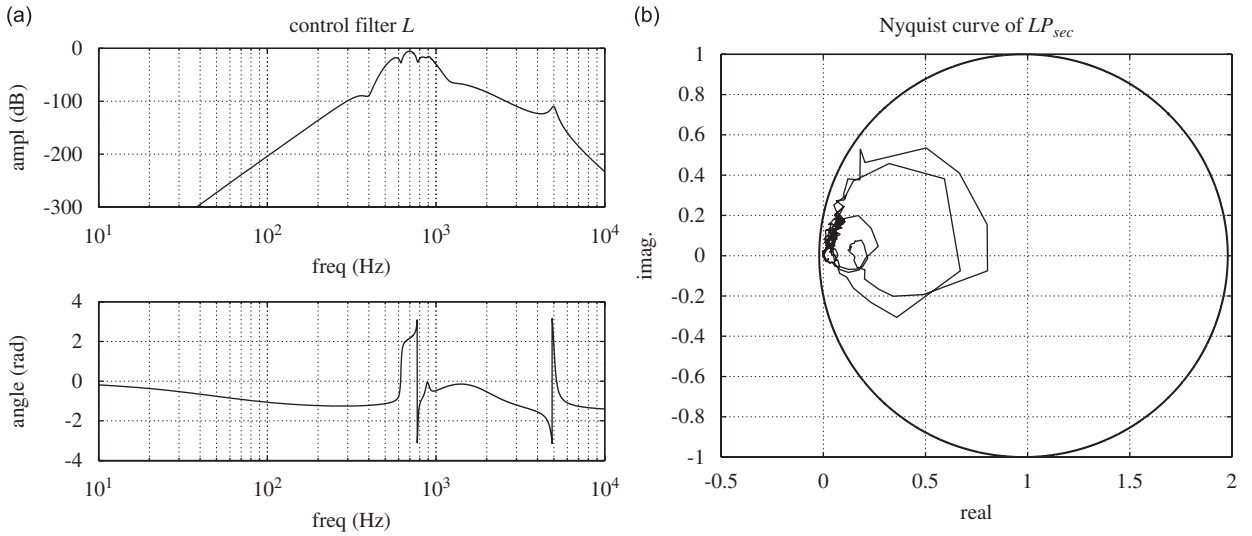

Fig. 12. The second part in the design of the ILC filter for the control of the optimal control configuration: (a) the transfer function of the total ILC control filter L and (b) the Nyquist plot of LP_{sec} inside the learning circle (the stability test for $q = 0.98$).

The gain of L is adjusted such that the maximum amplitude of LP_{sec} is close to 1 in the frequency range of interest. The transfer function of the resulting L-filter is shown in Fig. 12(a). Compared to the transfer function of L_2, there is no change of the phase due to the use of noncausal filters, such that the phase of LP_{sec} still stays between -90° and 90° between 500 and 900 Hz. However, the amplitude is strongly reduced below 500 Hz and above 900 Hz, generating the desired bandpass characteristic. If the same bandpass filtering of the amplitude would have been created by a causal filter, this would have caused a strong phase change over a broad frequency range, also between 500 and 900 Hz, the frequency range of interest. It is impossible to keep the phase of LP_{sec} between -90° and 90° in this latter range with a causal ILC controller, that generates the required bandpass characteristic of L. This bandpass filtering without a phase change is a great benefit of noncausal filters.

Based on the selected L-filter, the value q, which defines the Q-filter, is chosen. Since for a q-value of 1 the condition for monotonic convergence Eq. (16) is not fulfilled, q is reduced to 0.98. Fig. 12(b) shows that for this value of q the Nyquist curve of LP_{sec} does not exceed the learning circle, which guarantees monotonic convergence.

The theoretical reduction $|Y_\infty(e^{i\omega T})|/|P_{\mathrm{dist}}(e^{i\omega T})D(e^{i\omega T})|$, which can be achieved by the selected L- and Q-filter, is shown in Fig. 13. Contrary to the causal controller in the previous section, a high error reduction can be achieved by this noncausal ILC controller in the higher frequency range, where most of the noise is radiated. The error in the error accelerometer can be reduced by at least 10 dB over the whole frequency range of interest from 500 to 900 Hz. While the causal controller only reduces the error at the resonance peaks, the noncausal controller with a L-filter, which compensates all the zeros and poles of P_{sec}, creates a broadband vibration reduction at the error sensor: there is not only a reduction at the resonance frequencies but also at the intermediate frequencies.

The noncausal controller as discussed in the previous paragraphs has been implemented on a dSPACE 1103 DSP board and applied to the plate case study. A detailed survey of the practical implementation of a noncausal control filter can be found in Appendix A. In the remainder of this section, the local results, achieved by the noncausal controller at the error sensor, are studied. The influence of the controller on the global plate vibration level and the radiated acoustic noise level will be described in the next section.

The results, obtained by the noncausal controller at the error sensor in the plate experiments, are plotted in Figs. 14(a and b). Fig. 14(a) shows the error acceleration signals in the time domain, when the plate is excited by a primary impact force. The different curves compare the remaining error signals, which are obtained by the noncausal ILC algorithm after a different number of impacts. Since most of the vibration power in the error sensor is situated in the lower frequency range below 250 Hz and the greatest reduction is achieved

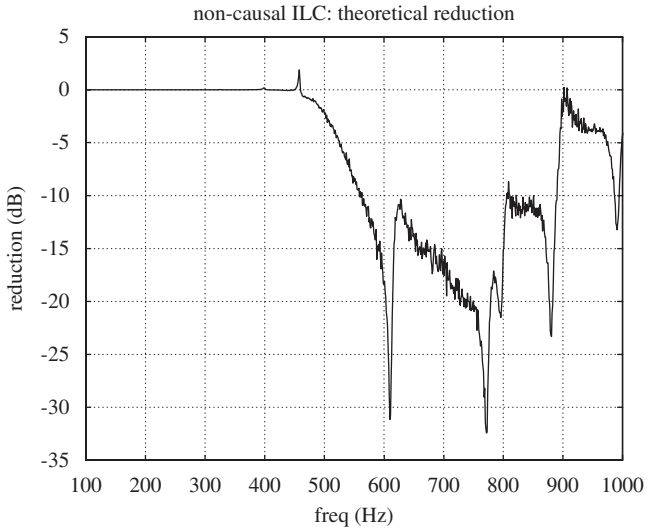

Fig. 13. The theoretical reduction $|Y_\infty(e^{i\omega T})|/|P_{dist}(e^{i\omega T})D(e^{i\omega T})|$, which can be achieved by the noncausal ILC controller.

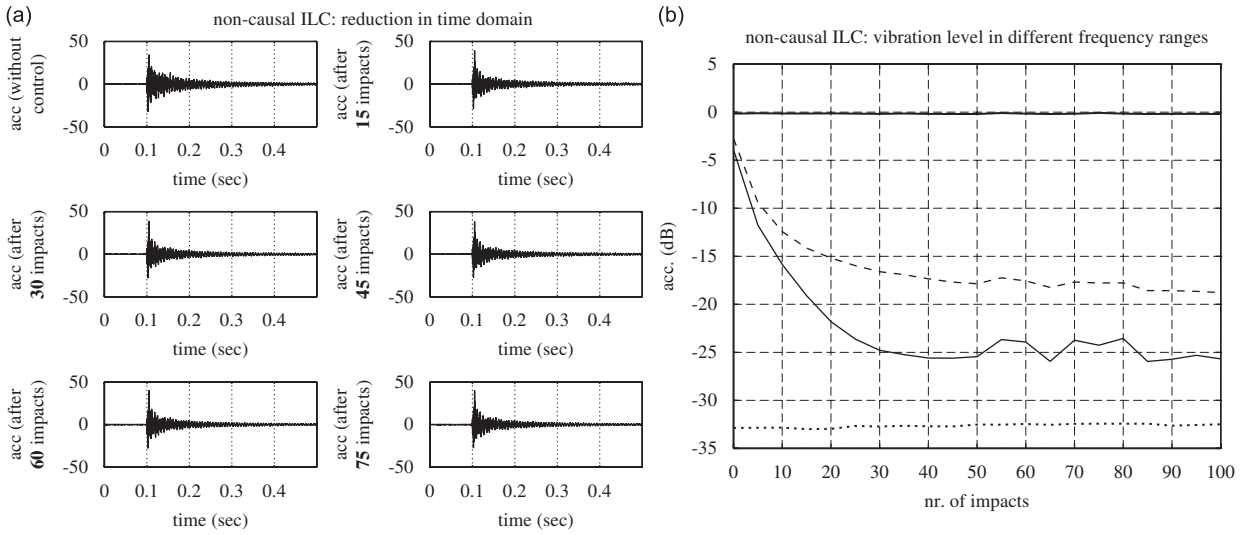

Fig. 14. The performance of the noncausal ILC controller: (a) the error acceleration after a certain number of learning impacts (shown in the time domain) and (b) the error acceleration as a function of the number of learning impacts (shown in different frequency bands: 50–250 Hz (bold line), 250–500 Hz (dotted line), 500–750 Hz (solid line) and 750–1000 Hz (dashed line)).

between 500 and 900 Hz, the reduction due to the learning process can hardly be detected in the time domain. However, the learning behaviour can clearly be observed in the frequency domain (Fig. 14(b)): in the frequency bands between 500 and 750 Hz and between 750 and 1000 Hz there is a clear reduction of more than 15 dB of the error signal during the first 50 impacts, while below 500 Hz the error signal has not changed. This is exactly the performance, which was theoretically predicted (Fig. 13). After the 50th impact, the learning behaviour of the ILC algorithm has converged and there is no further reduction.

5. Controller performance evaluation

This section discusses first the global performance (i.e. the total vibration level and the radiated noise level) of the implemented causal and noncausal algorithm. Afterwards the benefits of a controller, which combines

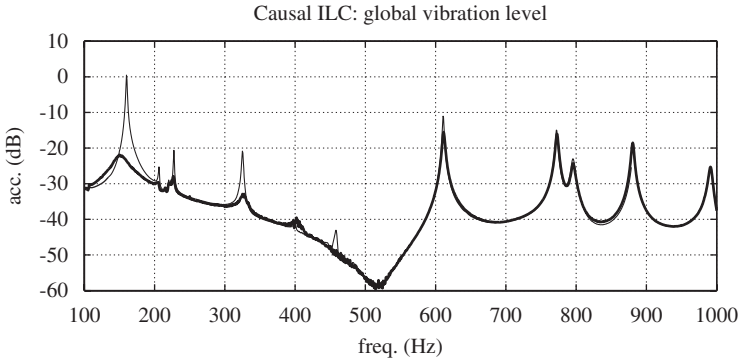

Fig. 15. The global vibration level of the whole plate without control (solid line) and with causal ILC/equivalent time-invariant feedback control (bold line).

both algorithms, are investigated. The global vibration level and the radiated noise level are measured, respectively, by 7 accelerometers, uniformly distributed over the plate and by 1 microphone in the far field (2 m from the plate). The global vibration level is defined as the rms-value of the accelerations measured by these 7 accelerometers.

5.1. Example 1: causal ILC

Since the reduction in the error sensor, which is achieved by the causal ILC algorithm after convergence, is the same as the reduction by the equivalent time-invariant feedback algorithm, the global performance of both controllers is also equal. Therefore, the results are only presented for the practically more feasible time-invariant feedback controller.

Fig. 15 shows the vibration levels of the plate without and with control. It is clear that in the lower frequency range below 500 Hz the resonance peaks are strongly damped by the causal controller. In the intermediate frequency ranges between the resonances, the global vibration level of the plate does not change, because the causal controller does not send a control signal to the secondary actuator in these frequency bands. Due to this controller design, a global vibration reduction of 10 dB is obtained between 100 and 500 Hz. In the higher frequency range above 500 Hz, the global vibration level is also not influenced by the causal controller due to the lowpass filter in the design of L and C_{FB}. The resulting overall reduction of the global plate vibrations is 5.5 dB. In Fig. 16, the A-weighted radiated noise levels are plotted in the one-third octave bands below 1000 Hz. Contrary to the global vibration level, the radiated noise levels are not significantly reduced in the lower frequency range, since the low-frequency modes of a non-baffled plate are not very efficiently radiating. Especially below 250 Hz, the radiated noise level hardly exceeds the background level. However, in the frequency band of 315 Hz, where the highest amount of low-frequency (<500 Hz) acoustic energy is radiated, there is a clear noise reduction of 5 dB. In the higher frequency range, only a small reduction of 3 dB can be observed in the one-third octave band of 630 Hz. Due to the limited radiation efficiency of the low-frequency modes, the global plate vibration reduction results only in a 1 dB(A) total noise reduction.

5.2. Example 2: noncausal ILC

This paragraph studies the global effect on the plate behaviour of the noncausal controller, developed in the previous section. Contrary to the causal ILC controller, which creates a low-frequency reduction, the noncausal controller focuses on a noise and vibration reduction in the higher frequency range (500–900 Hz), where most of the radiated noise is situated. Due to the introduction of the noncausal bandpass filter in the design of L, no control signal is sent to the secondary actuator below 500 Hz. This explains why the global vibration spectrum below 500 Hz with control is the same as the uncontrolled spectrum (Fig. 17). In the

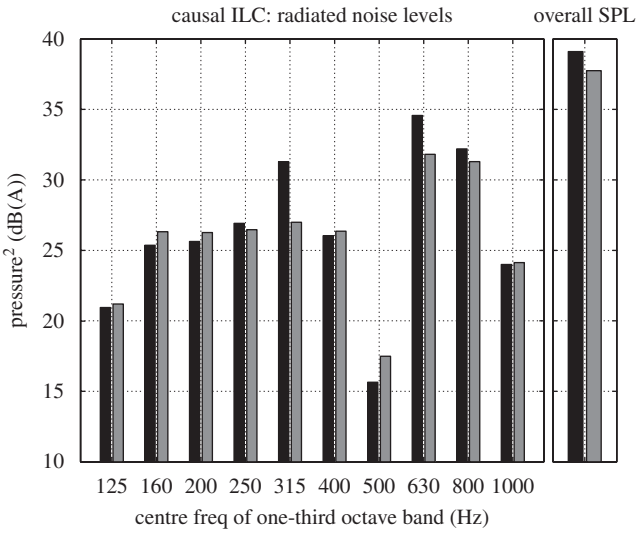

Fig. 16. The A-weighted radiated noise levels in the one-third octave bands below 1000 Hz and the A-weighted overall Sound Power Level without control (black) and with causal ILC (grey).

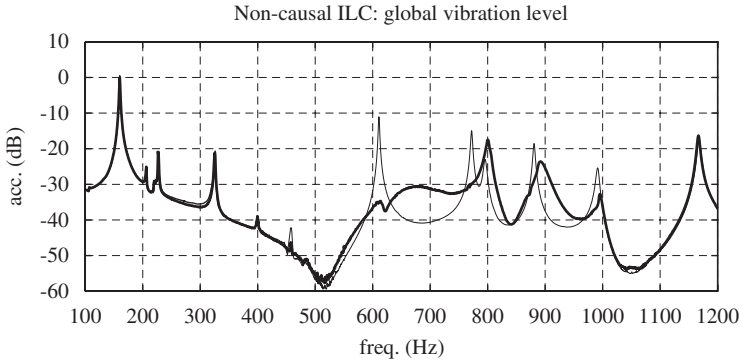

Fig. 17. The global vibration level of the whole plate without control (solid line) and with noncausal ILC (bold line).

previous section, Fig. 14(b) shows that between 500 and 1000 Hz the vibrations in the error sensor are significantly reduced by the control signal of the noncausal ILC controller. Due to the appropriate selection of the control configuration with successive poles in the plant transfer function P_{sec} (presented in Section 3), a vibration cancellation at the error sensor is supposed to result in a global vibration reduction. This reasoning is confirmed in Fig. 17: a vibration reduction of 1.5 dB is achieved by the noncausal ILC controller in the frequency band between 500 and 1000 Hz. Because the three most efficiently radiating plate modes at 611, 772 and 881 Hz are strongly damped, the noise reduction is more pronounced than the vibration reduction: a total noise reduction of 7 dB(A) is obtained between 500 and 1000 Hz. The noise reduction in one-third octave bands is presented in Fig. 18. The overall noise reduction over the whole frequency range is only 2.5 dB(A). This level is limited by the remaining low-frequency noise especially in the one-third octave band of 315 Hz, which is not tackled by the noncausal controller.

Since one zero (at 800 Hz) in the transfer function between the actuator and the sensor is inevitable in the frequency range 500–900 Hz (Fig. 3(b)), there is still 1 peak at this frequency in the global vibration level with control, which limits the vibration reduction. However, this vibration peak cannot be observed in the radiated noise (Fig. 18) because the corresponding vibration mode at this frequency is not an efficient noise radiator.

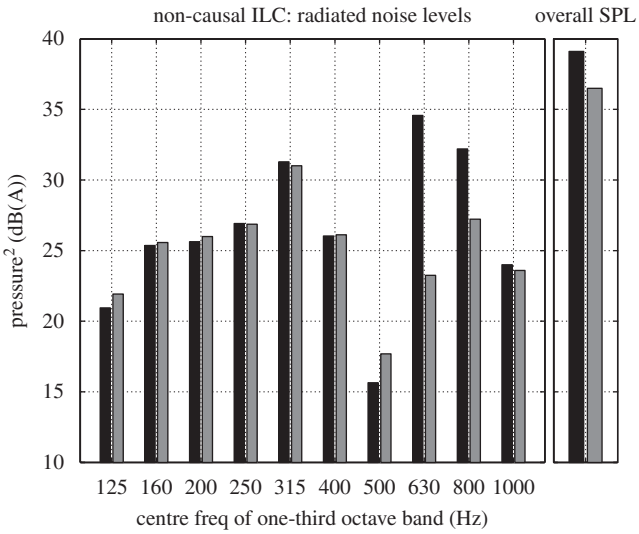

Fig. 18. The A-weighted radiated noise levels in the one-third octave bands below 1000 Hz and the A-weighted overall Sound Power Level without control (black) and with noncausal ILC (grey).

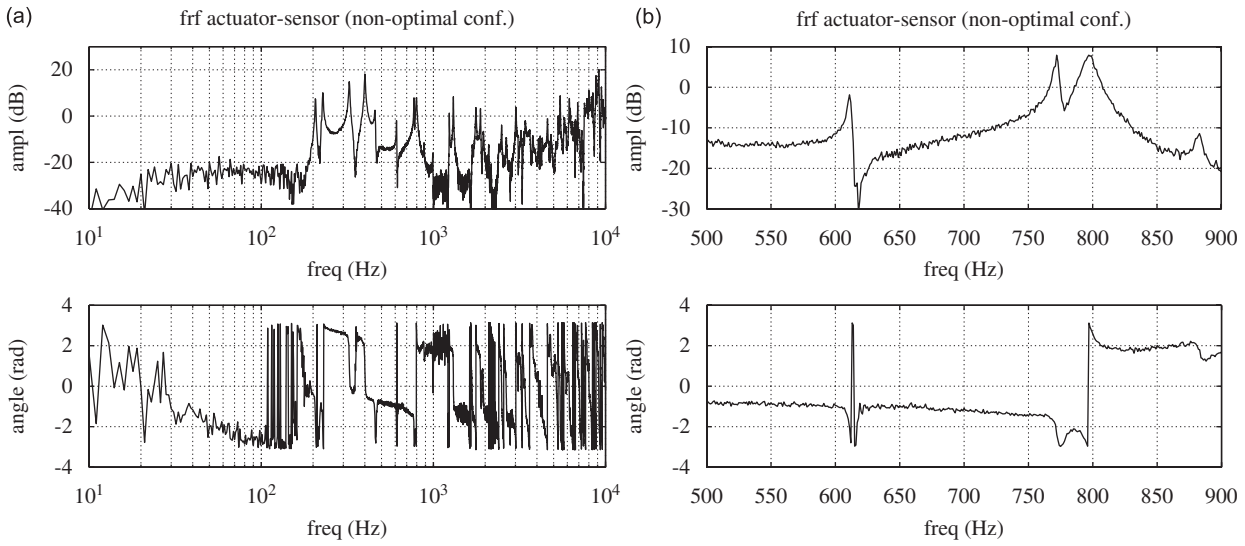

Fig. 19. The transfer function between the actuator force and the sensor (non-optimal control configuration): (a) over the whole frequency range and (b) in the frequency range 500–900 Hz, where the greatest noise reduction is required.

It is clear that due to the good selection of the actuator and sensor position a global vibration and noise reduction can be realized in the higher frequency domain. The cancellation of the disturbance in the optimal error sensor results in a global performance. Other configurations with the error sensor at different positions, which were not optimal (i.e. no successive poles in the secondary plant transfer function P_{sec}), were also experimentally tested. Noncausal ILC control filters were designed for all these new configurations. Although a disturbance rejection could be easily obtained at the new error sensors by the controllers, in all these cases, the local disturbance reduction resulted in a higher global vibration level than the level obtained by the optimal configuration.

One of those non-optimal control configurations is briefly discussed in the following paragraph. While the actuator is located in the same corner of the plate as in the previous examples, the error sensor is placed in the

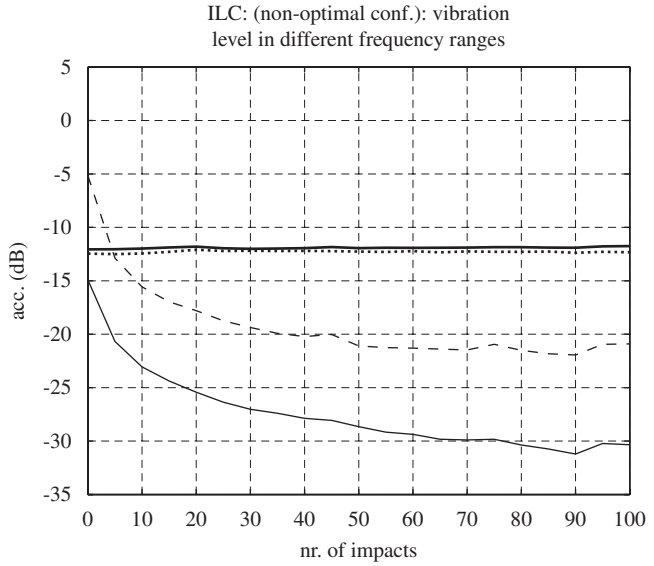

Fig. 20. The performance at the error sensor of the noncausal controller (for the non-optimal control configuration): the error acceleration as a function of the number of learning impacts (shown in different frequency bands: 50–250 Hz (bold line), 250–500 Hz (dotted line), 500–750 Hz (solid line) and 750–1000 Hz (dashed line)).

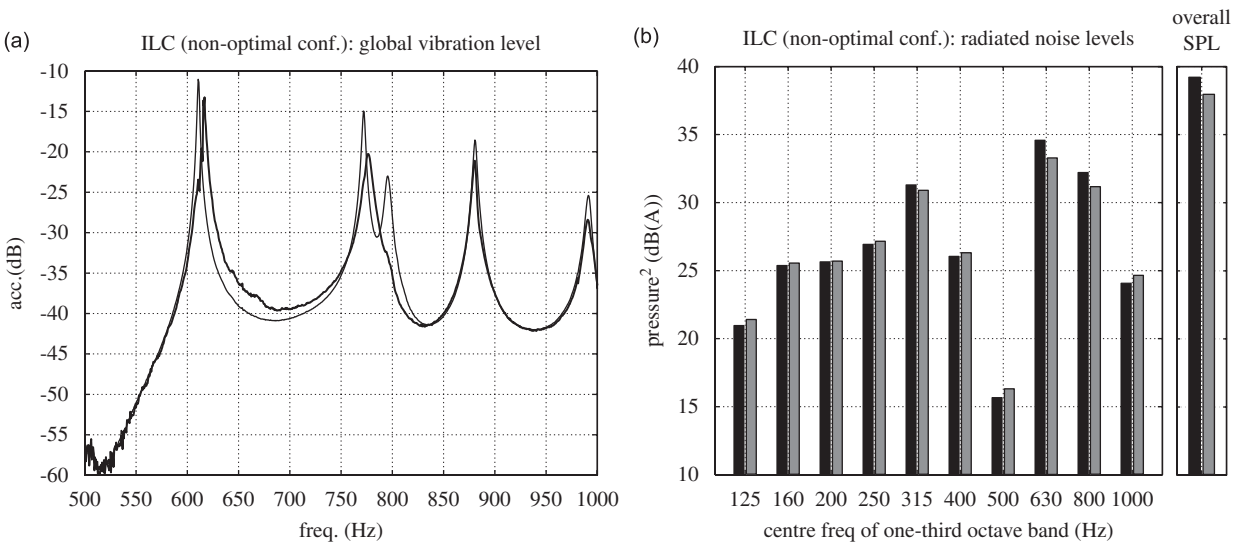

Fig. 21. The global performance achieved by a controller for the non-optimal control configuration: (a) the global vibration level of the whole plate without control (solid line) and with noncausal ILC (bold line) and (b) the A-weighted radiated noise levels in the one-third octave bands below 1000 Hz and the A-weighted overall Sound Power Level without control (black) and with noncausal ILC (grey).

middle of the plate's lower part. Figs. 19(a and b) show the transfer function of the secondary plant P_{sec} between this actuator and sensor: it is clear that two zeros with limited damping (at 620 and 778 Hz) occur in this transfer function, which is not optimal according to the procedure for the selection of the configuration developed in Section 3.

In a similar way as in Section 4.3.2 a noncausal controller is developed for this non-optimal control configuration. The performance of the designed controller at the error sensor is plotted in Fig. 20: after convergence of the ILC algorithm a strong reduction is obtained in the frequency range of interest between

500 and 900 Hz. Although the vibration level at the error sensor is significantly reduced in this frequency band, the global vibration level (Fig. 21(a)) and the radiated noise level (Fig. 21(b)) have hardly decreased. Due to the zeros in the plant transfer function P_{sec} at 620 and 778 Hz, a high control force is necessary to cancel the vibrations at the error sensor at these frequencies. However, since a zero is not a global property of the plate, this high control force creates high vibration levels at the greater part of the plate such that the global vibration level and the radiated noise level are significantly amplified around 620 and 778 Hz. The reduction achieved by the controller at other frequencies is almost completely cancelled by the amplification at those 2 frequencies, which explains why no significant global performance can be obtained.

5.3. Example 3: combined time-invariant feedback and ILC controller

The residual noise, which cannot be cancelled out by the noncausal controller in the second example, has a predominant low-frequency character. This low-frequency noise can be suppressed by the addition of a causal ILC controller or its equivalent time-invariant feedback controller, as presented in the first example. Therefore a control system, consisting of a time-invariant feedback controller combined with a noncausal ILC controller, is designed for the plate. The control scheme of this controller is presented in Fig. 22. The control signal u_i to the secondary actuator consists of a signal $u_{i,\mathrm{fb}}$ from the causal feedback control filter and a signal $u_{i,\mathrm{ILC}}$ from the ILC controller. The feedback part of the combined controller, which uses a collocated error sensor in the corner of the plate (measuring $y_{i,\mathrm{fb}}$), uses the same control filter C_{fb} as in the first example. This controller reduces the low-frequency noise, compensates for repetitive as well as random disturbances and is immediately effective at the first controlled impact without a learning process. The noncausal ILC part of the controller is only used to reduce the residual high-frequency error, that cannot be controlled by the time-invariant feedback controller C_{fb}. The error signal for this noncausal controller $y_{i,\mathrm{ILC}}$ is measured by a second error sensor, which is located at the optimal position to achieve global reduction: this position is identical to the optimal location defined in the second example. The development of the noncausal ILC controller (control filters Q and L) is performed in the same way as for the noncausal controller without feedback. However, the controllable plant is now $P_{\mathrm{ILC}}/1 + C_{\mathrm{fb}}P_{\mathrm{fb}}$ instead of P_{ILC}, where P_{fb} and P_{ILC} are the two transfer functions between the actuator force in the corner of the plant and the responses in the error sensors, respectively.

Fig. 23 shows the vibration levels measured by the second error sensor (measuring $y_{i,\mathrm{ILC}}$) in 4 frequency bands below 1000 Hz during the first 100 impacts. The behaviour in the 2 frequency bands below 500 Hz differs significantly from the 2 bands above 500 Hz. Below 500 Hz, the time-invariant feedback controller is mainly active, such that no learning behaviour can be observed. The final reduction is already obtained after the first controlled impact. Above 500 Hz, the control signal from the time-invariant feedback controller strongly decreases due to the lowpass filter in the control design. In this frequency range, however, the ILC controller becomes active and will determine the control performance. In the frequency bands 500–750 Hz and 750–1000 Hz, the vibration level decreases gradually at every impact due to the learning process in the ILC

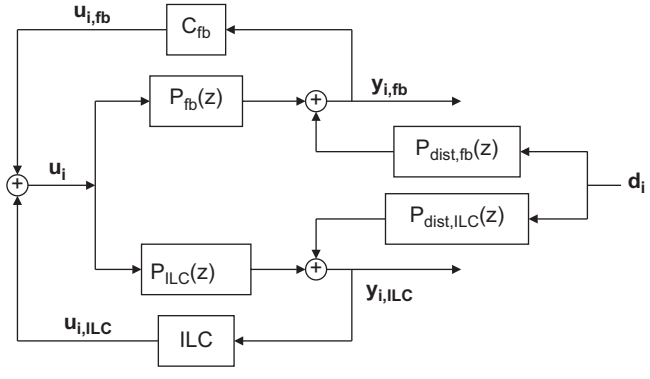

Fig. 22. Control scheme of the combined feedback/ILC controller.

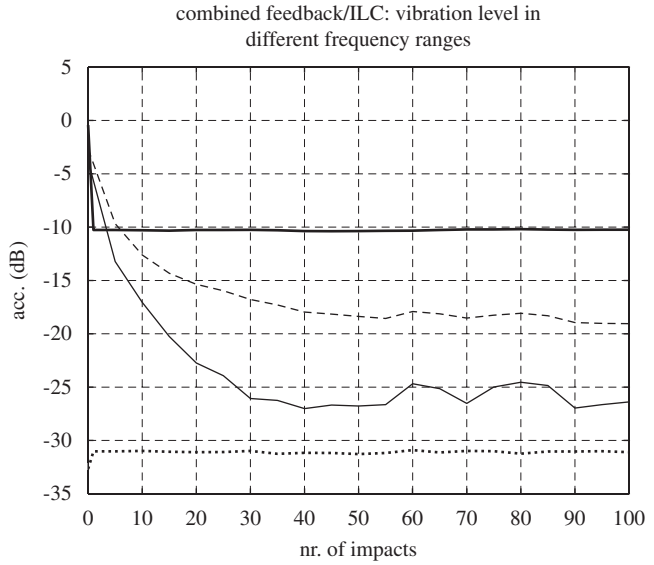

Fig. 23. The performance of the combined feedback/ILC controller at the error sensor, which measures $y_{i,\mathrm{ILC}}$: the error acceleration as a function of the number of learning impacts (shown in different frequency bands: 50–250 Hz (bold line), 250–500 Hz (dotted line), 500–750 Hz (solid line) and 750–1000 Hz (dashed line)).

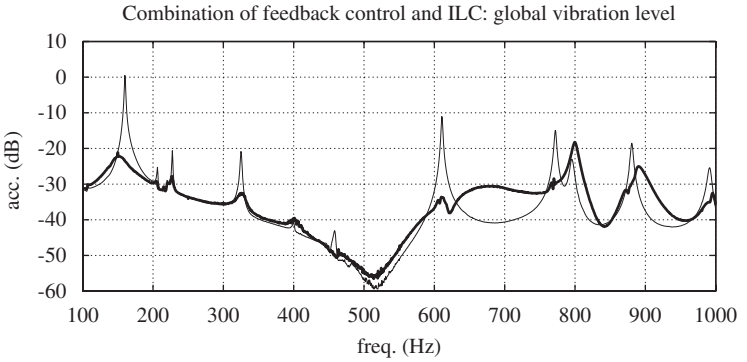

Fig. 24. The global vibration level of the whole plate without control (solid line) and with combined feedback/ILC control (bold line).

algorithm. After 50 impacts, there is no further reduction, which indicates that the ILC controller has converged.

The global performance of this combined controller after convergence is also measured and compared to the two other controllers. The global vibration reduction of this controller is plotted in Fig. 24. It is clear that the new controller combines the benefits of the 2 previous controllers: a vibration reduction is achieved in the lower as well as in the higher frequency range. This results in a broadband global vibration reduction of 6 dB. Fig. 25 shows the noise reduction in the one-third octave bands below 1000 Hz without and with feedback/ILC control. In the 3 one-third octave bands, where the plate radiates the highest noise levels (315, 630 and 800 Hz), significant noise reductions are obtained by this combined controller such that the total noise level is reduced by 3.5 dB(A).

6. Conclusions

In this paper, a design strategy is proposed for the development of an ASAC system to reduce repetitive structural impact noise. The design process is divided into two parts: first the optimal control configuration is

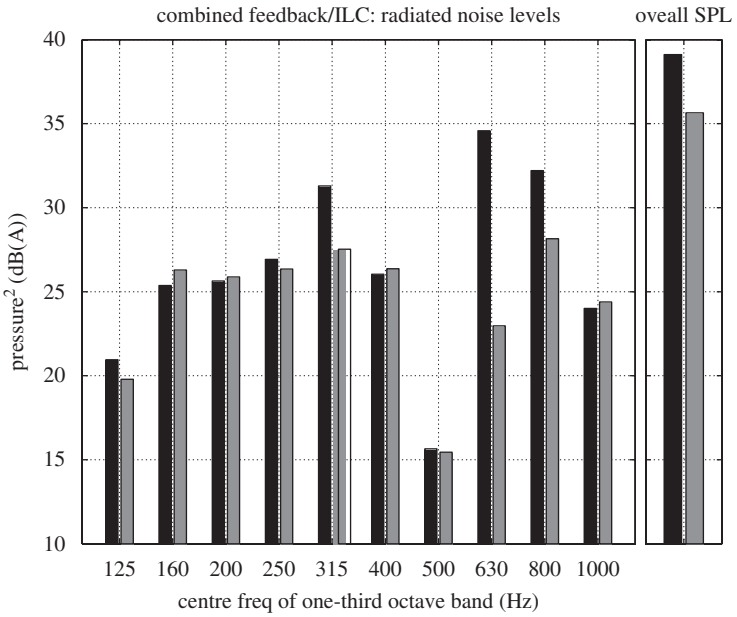

Fig. 25. The A-weighted radiated noise levels in the one-third octave bands below 1000 Hz and the A-weighted overall Sound Power Level without control (black) and with the combined feedback/ILC controller (grey).

defined and afterwards a control algorithm is implemented for the selected actuator(s) and sensor(s). To find the optimal actuator and sensor locations, a selection procedure is developed such that the chosen control system will create a high global vibration and noise reduction in case of a perfect disturbance cancellation at the error sensors. Since an impact generates a broadband excitation, most of the noise will be radiated at certain structural resonance frequencies. Therefore in the optimal configuration for impact noise control the global vibrations are strongly reduced at these resonance frequencies without significantly amplifying the vibration levels in the intermediate frequency ranges.

In the second step of the ASAC design process, a control algorithm is developed for the selected optimal configuration. This algorithm defines the achievable reduction of the vibrations at the error sensors and consequently the possible global noise and vibration reduction. Because in many industrial applications, where the reduction of impact noise is an issue, successive impacts have a repetitive behaviour, this repetitiveness can be used in the design of the control algorithms. Causal and noncausal ILC controllers, which use knowledge from the previous impacts to calculate the control signal for the next impact, are presented and compared to traditional time-invariant feedback algorithms. While equivalent feedback controllers exist for causal ILC systems, this is not the case for noncausal ILC systems. Therefore, the benefits of noncausal ILC algorithms (i.e. much more freedom in the design of the ILC filters) are extensively explored in this paper. The efficiency of the whole design methodology has been verified in a practical example, where an ASAC system is developed to reduce the low frequency (<1000 Hz) impact noise radiated by a plate. The same methodology can however also be used for the active reduction of higher frequency noise, if the higher frequency content of the successive impacts is sufficiently repetitive.

The future work consists of a theoretical and a practical part. In the first part, the possibilities of noncausal ILC algorithms will be further investigated. For example, different noncausal algorithms, each focussing on a certain frequency range, will be implemented in parallel in order to get a good performance over a broader frequency range. The second part focuses on the application of the developed methodology on real industrial machinery (e.g. punching machines, presses, etc.). In these industrial noise problems, additional challenges can be expected: the influence of the limited repetitiveness of the successive impacts has to investigated; a proper trigger signal, which announces a new impact accurately, has to be searched; probably new actuators and sensors, which can deliver and measure a high amount of energy during short periods, will be necessary; etc.

However, provided these practical problems can be resolved, the good results, achieved with the presented design methodology of ASAC systems, are very promising for the use in industrial impact noise applications.

Acknowledgements

The research of G. Pinte is financed by a scholarship of the Institute for the Promotion of Innovation through Science and Technology in Flanders (IWT Vlaanderen). A part of this research is also funded by the European research project Noiseless.

Appendix A. Implementation of noncausal filters

The response $y(t)$ of a linear time-invariant (LTI) noncausal system can be calculated by the convolution of the input signal $x(t)$ and the impulse response $h(t)$ of the system:

$$y(t) = \int_{-\infty}^{+\infty} x(\tau)h(t-\tau)\,\mathrm{d}\tau \tag{A.1}$$

The two-sided Laplace transform of the impulse response function $h(t)$ is defined as

$$H(s) = \int_{-\infty}^{+\infty} h(t)\mathrm{e}^{-st}\,\mathrm{d}t \tag{A.2}$$

for all $s \in \mathbb{C}$, for which the above integral converges.

Two spaces can be distinguished depending on the causality of the LTI operator. While a transfer function with poles in the open left half-plane corresponds to a stable causal system, a transfer function with poles in the open right half-plane defines a stable anti-causal system, i.e. the impulse response $h(t)$ is equal to 0 for $t>0$. For example, $H(s) = 1/s^2 - 2\times 0.1(2\pi 600)s + (2\pi 600)^2)$ is the two-sided Laplace transform of the stable, anti-causal system with the following impulse response:

$$h(t) = \begin{cases} -\dfrac{1}{2\pi 600\sqrt{1-0.1^2}}\mathrm{e}^{2\pi 600\times 0.1t}\sin(2\pi 600\sqrt{1-0.1^2}t) & \text{for } t<0 \\ 0 & \text{for } t\geqslant 0 \end{cases} \tag{A.3}$$

Consider an anti-causal LTI system H_{anticaus} with an impulse response $h_{\text{anticaus}}(t)$, which processes an input signal $x(t)$ to calculate the output $y(t)$. Define the equivalent causal LTI system $H_{\text{caus,eq}}$ with the impulse response $h_{\text{caus,eq}}(t)$, which is the reverse of $h_{\text{anticaus}}(t)$:

$$h_{\text{caus,eq}}(t) = h_{\text{anticaus}}(-t) \tag{A.4}$$

The two-sided Laplace transform $H_{\text{caus,eq}}(s)$ of the equivalent causal system equals

$$\begin{aligned} H_{\text{caus,eq}}(s) &= \int_{-\infty}^{+\infty} h_{\text{caus,eq}}(t)\mathrm{e}^{-st}\,\mathrm{d}t \\ &= \int_{-\infty}^{+\infty} h_{\text{anticaus}}(-t)\mathrm{e}^{-st}\,\mathrm{d}t \\ &= -\int_{+\infty}^{-\infty} h_{\text{anticaus}}(r)\mathrm{e}^{sr}\,\mathrm{d}r \\ &= \int_{-\infty}^{+\infty} h_{\text{anticaus}}(r)\mathrm{e}^{-(-s)r}\,\mathrm{d}r \\ &= H_{\text{anticaus}}(-s) \end{aligned} \tag{A.5}$$

Define the signals $x_{\text{rev}}(t)$ and $y_{\text{rev}}(t)$ as the reverse of the signals $x(t)$ and $y(t)$:

$$x_{\text{rev}}(t) = x(-t) \tag{A.6}$$

$$y_{\text{rev}}(t) = y(-t) \tag{A.7}$$

Using Eq. (A.1), $y_{\mathrm{rev}}(t)$ can be calculated:

$$\begin{aligned} y_{\mathrm{rev}}(t) &= y(-t) \\ &= H_{\mathrm{anticaus}}(x(-t)) \\ &= \int_{-\infty}^{+\infty} x(\tau) h_{\mathrm{anticaus}}(-t-\tau)\,\mathrm{d}\tau \\ &= \int_{-\infty}^{+\infty} x_{\mathrm{rev}}(-\tau) h_{\mathrm{anticaus}}(-t-\tau)\,\mathrm{d}\tau \end{aligned} \tag{A.8}$$

Since h_{anticaus} is anticausal, $h_{\mathrm{anticaus}}(-t-\tau)=0$ for $\tau<-t$:

$$\begin{aligned} y_{\mathrm{rev}}(t) &= \int_{-t}^{+\infty} x_{\mathrm{rev}}(-\tau) h_{\mathrm{anticaus}}(-t-\tau)\,\mathrm{d}\tau \\ &= -\int_{t}^{-\infty} x_{\mathrm{rev}}(\eta) h_{\mathrm{anticaus}}(\eta-t)\,\mathrm{d}\eta \\ &= \int_{-\infty}^{t} x_{\mathrm{rev}}(\eta) h_{\mathrm{anticaus}}(\eta-t)\,\mathrm{d}\eta \\ &= \int_{-\infty}^{t} x_{\mathrm{rev}}(\eta) h_{\mathrm{caus,eq}}(t-\eta)\,\mathrm{d}\eta \end{aligned} \tag{A.9}$$

Since $h_{\mathrm{caus,eq}}$ is causal, $h_{\mathrm{caus,eq}}(t-\eta)=0$ for $t<\eta$:

$$\begin{aligned} y_{\mathrm{rev}}(t) &= \int_{-\infty}^{+\infty} x_{\mathrm{rev}}(\eta) h_{\mathrm{caus,eq}}(t-\eta)\,\mathrm{d}\eta \\ &= H_{\mathrm{caus,eq}}(x_{\mathrm{rev}}(t)) \end{aligned} \tag{A.10}$$

This derivation proves the principle, which is used for the calculation of the output of an anti-causal operator H_{anticaus}. The scheme of the calculation procedure is shown in Fig. 26. The equivalent causal operator $H_{\mathrm{caus,eq}}$, which can be calculated according to Eq. (A.5), is applied on the reverse of the input signal. The result of this operation is then the reverse of the desired output.

As an example, the equivalent causal filter is calculated for the anti-causal system, described by Eq. (A.3):

$$\begin{aligned} H_{\mathrm{caus,eq}}(s) &= H_{\mathrm{anticaus}}(-s) \\ &= \frac{1}{(-s)^2 - 2\times 0.1(2\pi 600)(-s) + (2\pi 600)^2} \\ &= \frac{1}{s^2 + 2\times 0.1(2\pi 600)s + (2\pi 600)^2} \end{aligned} \tag{A.11}$$

In Figs. 27(a and b) the impulse response as well as the Laplace transform of the anti-causal and the equivalent causal system are compared. It is clear that the impulse responses of both filters are symmetric, which explains why the anti-causal filter can be replaced by the equivalent causal filter. The Bode plot of the filters (Fig. 27(b)) shows that the amplitude of both filters is equal. However, in the anti-causal filter the decrease of the amplitude introduces a phase lead of 180° while in the equivalent causal filter a phase lag of 180° is present. This is also the reason why the equivalent causal and the anti-causal filter were combined in the design of the *L*-filter to create a bandpass filter without a change of the phase.

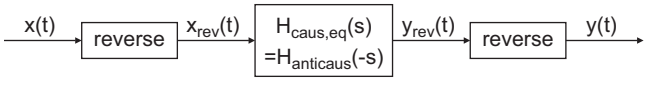

Fig. 26. The procedure to calculate the output of an anti-causal filter H_{anticaus}.

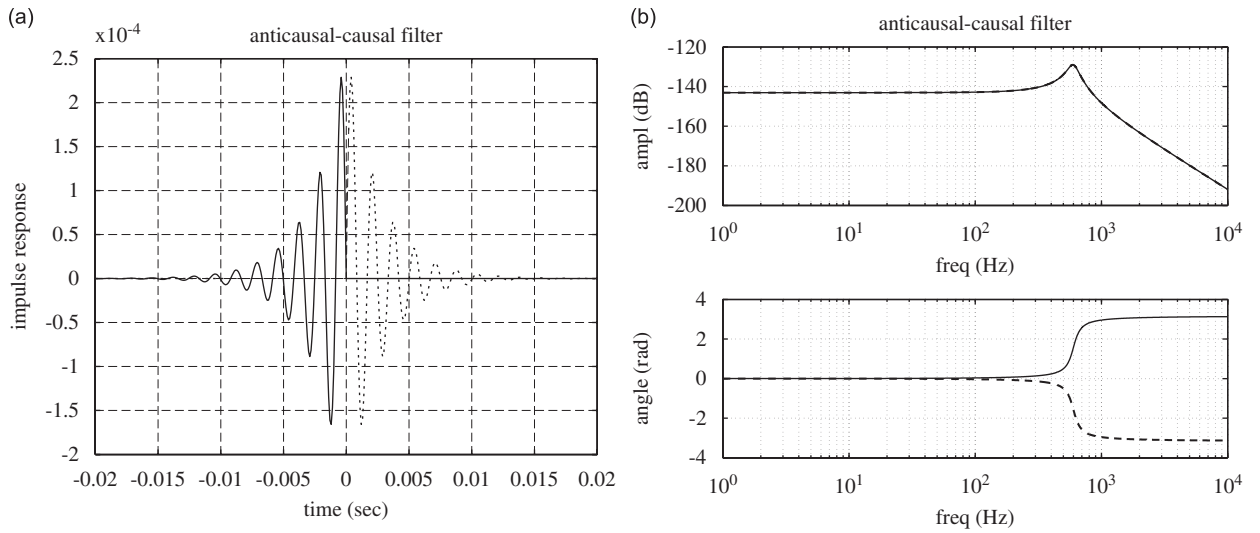

Fig. 27. A second-order anti-causal filter (solid line) and the equivalent causal filter (dotted/dashed line): (a) the impulse response and (b) the Bode plot of both filters.

The impulse response $h(t)$ of a general noncausal LTI system can differ from 0 for negative as well as for positive time values. Such a noncausal system can be considered as the combination of a causal system and an anti-causal system: the system can be implemented either as a sum or a product of causal and anti-causal operators. In this application, the control filter L is developed as a product of operators with causal and anti-causal poles and zeros. Therefore, in the implementation of this filter, the input signal $\underline{y}$ is successively processed first by all the causal and afterwards by all the anti-causal operators.

References

[1] A. Akay, A review of impact noise, *Journal of the Acoustical Society of America* 64 (4) (1978) 977–987.
[2] E.J. Richards, A. Lenzi, On the prediction of impact noise, IX: the noise from punch presses, *Journal of Sound and Vibration* 103 (1) (1985) 43–81.
[3] W. Dehandschutter, *The Reduction of Structure-borne Noise by Active Vibration Control*, Dissertation, KU Leuven, Leuven, Belgium, 1997.
[4] P. Gardonio, S. Elliott, Smart panels for active structural acoustic control, *Smart Materials and Structures* 13 (6) (2004) 1314–1336.
[5] S. Elliott, *Signal Processing for Active Control*, Academic Press, London, UK, 2001.
[6] X. Sun, S.M. Kuo, G. Meng, Adaptive algorithm for active control of impulsive noise, *Journal of Sound and Vibration* 291 (2) (2006) 516–522.
[7] R.L. Clark, D.S. Bernstein, Hybrid control: seperation in design, *Journal of Sound and Vibration* 214 (4) (1998) 784–791.
[8] N. Doelman, A unified control strategy for the active reduction of sound and vibration, *Journal of Intelligent Material Systems and Structures* 2 (1991) 558–580.
[9] G. Pavic, Comparison of different strategies of active vibration control, *Proceedings of ACTIVE 95*, Newport Beach, CA, USA, 1995.
[10] J. Pan, C.H. Hansen, Active control of total vibratory power flow in a beam. I: physical system analysis, *Journal of the Acoustical Society of America* 89 (4) (1991) 200–209.
[11] R.L. Clark, C.R. Fuller, Optimal placement of piezoelectric actuators and polyvinylidene fluoride error sensors in active structural acoustic control approaches, *Journal of the Acoustical Society of America* 92 (3) (1992) 1521–1533.
[12] O. Bardou, P. Gardonio, S.J. Elliott, R.J. Pinnington, Active power minimisation and power absorption in a plate with force and moment excitation, *Journal of Sound and Vibration* 208 (1) (1997) 111–151.
[13] M.H.H. Oude Nijhuis, A. de Boer, Optimization strategy for actuator and sensor placement in active structural acoustic control, in: *Proceedings of ACTIVE 2002*, Southampton, UK, 2002.
[14] D.C. Zimmerman, A Darwinian approach to the actuator number and problem placement with non negligible actuator mass, *Mechanical Systems and Signal Processing* 7 (4) (1993) 363–374.
[15] V.V. Varadan, J. Kim, V.K. Varadan, Optimal placement of piezoelectric actuators for active noise control, *AIAA Journal* 35 (3) (1997) 526–533.

[16] D.A. Bristow, M. Tharayil, A.G. Alleyne, A survey of iterative learning control, *IEEE Control Systems Magazine* 26 (3) (2006) 96–114.
[17] M. Uchiyama, Formulation of high-speed motion pattern of mechanical arm by trial, *Transactions of the Society of Instrumentation and Control Engineers* 19 (1978) 706–712.
[18] S. Arimoto, S. Kawamura, F. Miyazaki, Bettering operation of robots by learning, *Journal of Robotic Systems* 1 (1984) 123–140.
[19] S. Arimoto, S. Kawamura, F. Miyazaki, Iterative learning control for robot systems, *Proceedings of IECON*, Tokyo, Japan, 1984.
[20] R.W. Longman, Iterative learning control and repetitive control for engineering practice, *International Journal of Control* 73 (10) (2000) 930–954.
[21] R. Horowitz, Learning control of robot manipulators, *ASME Journal of Dynamic Systems Measurement and Control* 115 (2B) (1993) 402–411.
[22] K.L. Moore, *Iterative Learning Control for Deterministic Systems*, Springer, London, UK, 1993.
[23] K.L. Moore, Iterative learning control: an expository overview, *Applied and Computational Controls, Signal Processing, and Circuits* 1 (1) (1998).
[24] P.B. Goldsmith, On the equivalence of causal LTI iterative learning control and feedback control, *Automatica* 38 (2002) 703–708.
[25] G. Pinte, W. Desmet, P. Sas, Active control of repetitive transient noise, *Journal of Sound and Vibration* 207 (3–5) (2007) 513–526.
[26] G. Pinte, W. Desmet, P. Sas, Active structural acoustic control of impact noise, *Proceedings of ISMA 2004*, Leuven, Belgium, 2004.
[27] Z. Bien, K.M. Huh, Higher-order iterative learning control algorithm, *IEEE Proceedings Part D, Control Theory and Applications* 136 (1989) 105–112.
[28] M. Norrlöf, S. Gunnarsson, A frequency domain analysis of a second order iterative learning control algorithm, in: *Proceedings of 38th IEEE Conference on Decision and Control*, Phoenix, AZ, USA, 1999.
[29] M. Norrlöf, Iterative Learning Control: Analysis, Design, and Experiments, Dissertation no. 653, Linköping Studies in Science and Technology, Sweden, 2000.
[30] M.H.A. Verwoerd, Iterative Learning Control—A Critical Review, Dissertation, University of Twente, Enschede, The Netherlands, 2005.